

The Importance of Initial Conditions in Seasonal Predictions of Antarctic Sea Ice

Elio Campitelli^{1, 2}, Ariaan Purich^{1, 2}, Julie Arblaster^{1, 2}, Eun-Pa Lim³, Matthew C. Wheeler³, and Phillip Reid³

¹School of Earth, Atmosphere and Environment, Monash University, Kulin Nations, Clayton, Victoria, Australia.

²ARC Special Research Initiative for Securing Antarctica's Environmental Future, Clayton, Kulin Nations, Victoria, Australia.

³Research, Bureau of Meteorology, Melbourne, Australia.

Correspondence: Elio Campitelli (elio.campitelli@monash.edu)

Abstract. Accurate Antarctic sea-ice forecasts are crucial for climate monitoring and operational planning, yet they remain challenging due to model biases and complex ice-ocean-atmosphere interactions. The two versions of the Australian Bureau of Meteorology's ACCESS seasonal forecast system, ACCESS-S1 and ACCESS-S2, use identical model configuration and differ only in their initial conditions; primarily in that ACCESS-S2 does not assimilate sea-ice observations, whereas ACCESS-S1 does.

This provides a convenient opportunistic experiment to assess the role of initial conditions on Antarctic sea-ice forecasts using more than 20 years of fully coupled simulations with two 9-member ensembles. Our analysis reveals that both systems experience an extended melt season and delayed growth phase compared with observations. This leads to a significant negative sea-ice extent bias, which is corrected only in ACCESS-S1 by the data assimilation system. The impact of the differing initial conditions on forecast errors varies dramatically by season: summer and autumn initial conditions (January-April) provide predictive skill for up to three months, with February initial conditions being particularly crucial. In contrast, winter forecasts of the two systems are statistically indistinguishable after only two weeks. Regional analysis of forecast skill suggests that this winter predictability barrier is most dramatic over East Antarctica, where even ACCESS-S1 shows negative skill. These findings highlight the critical importance of comprehensive year-round sampling in predictability studies and suggest that operational sea-ice data assimilation efforts should prioritise the summer-autumn period when initial conditions have maximum impact on forecast skill.

1 Introduction

Accurately modelling Antarctic sea ice is essential for understanding processes and improving climate projections to inform adaptation strategies. Accurate seasonal to sub-seasonal forecasts are also crucial for operation contingency planning in and around the Antarctic continent, including scientific missions, fisheries, and tourism (De Silva et al.,

2020; Wagner et al., 2020). Improvements in modelled sea-ice might also help improve weather forecasts over and away from sea-ice regions (Rinke et al., 2006; Wang et al., 2024; Semmler et al., 2016).

However, progress in Antarctic sea-ice forecasting system has lagged behind Arctic sea-ice forecasts due to model biases, and inherent large variability and complexity (Zampieri et al., 2019; Gao et al., 2024). Dynamical seasonal forecasts of summer Antarctic sea ice have been shown to perform worse than relatively simpler statistical methods (Massonnet et al., 2023) and machine learning approaches (e.g. Dong et al. (2024), Lin et al. (2025)), which also underscores the need for better understanding and physical modelling of sea-ice dynamics, and drivers of its variability.

Good initial conditions are generally required for a good forecast, however, it is not entirely known to what extent accurate sea-ice initial conditions affect the quality of the forecast and at what timescales. Exploring seasonal predictions of Arctic sea ice, Guemas et al. (2016) found that sea-ice initial conditions are important in autumn to predict summer sea ice, but the impact wasn't as dramatic when predicting winter sea ice. Day et al. (2014) also found seasonally-varying differences in the effect of initialisation, noting that accurate Arctic sea-ice thickness leads to improved sea-ice forecasts initialised in July but not when initialised in January.

For the Antarctic, Holland et al. (2013) studied the initial-value predictability of Antarctic sea ice in a perfect model study using the CCSM3 model. They found that sea-ice and ocean initial conditions provide predictive information to forecast sea-ice edge location several months in advance and that some predictability is retained for up to two years thanks to ocean heat content anomalies that are advected eastward. This is in contrast with Marchi et al. (2020), who ran perfect model experiments to argue that uncertainty in the predicted atmospheric state and evolution is the main driver of uncertainty in Antarctic sea-ice extent prediction on seasonal timescales, with sea-ice and ocean initial conditions having lesser importance. More recently, Morioka et al. (2022) studied decadal forecasts of Antarctic sea ice and found that initialising ocean and sea ice improved the correlation between simulated and observed sea-ice concentration evolution in the Amundsen–Bellingshausen Sea. It is hard to compare these studies since they are based on forecasts initialised at different times of the year and different frameworks: Holland et al. (2013) ran 20 ensemble members initialised on the 1st of January of a particular year, Marchi et al. (2020) ran forecasts from the 1st of March and 1st of September, and Morioka et al. (2022) ran forecasts only from the 1st of March. Marchi et al. (2020) also used a coupled ocean–sea-ice model instead of a fully coupled model like Holland et al. (2013) did. Morioka et al. (2022) used observed sea-ice initial conditions and compared with observations, while Marchi et al. (2020) and Holland et al. (2013) were perfect model studies.

In October 2021 the Australian Bureau of Meteorology (BoM) upgraded the Australian Community Climate and Earth System Simulator – Seasonal (ACCESS-S) from version S1 to S2. While the base model remained the same, the change in version was focused on using ocean, sea-ice and land initial conditions generated by the BoM instead of depending on the UK Met Office. Crucially, compared to ACCESS-S1, ACCESS-S2 does not assimilate sea-ice observations, so sea ice is only affected by the ocean and atmospheric data assimilation via the coupled integration.

Since model configuration is identical between ACCESS-S1 and ACCESS-S2, they form a sort of “opportunistic experiment” where the same forecasting model was run over a long period of time with multiple ensemble forecasts initialised throughout the year, with the only difference being the initial conditions. This provides an opportunity to test the effect of sea-ice initial conditions on the forecast of sea-ice concentrations and the climate.

In this study we compare sea-ice hindcasts produced by ACCESS-S1 and ACCESS-S2. We focus on seasonality of errors and biases and the effect of the data assimilation system. This comparison will inform future work with the prediction system as a research tool to better understand the dynamics and variability of the Antarctic sea ice and its impacts on the climate system as well as to explore the potential of using its sea-ice forecasts for decision-making. The work will also serve as a benchmark for future prediction systems to attempt to improve upon.

2 Data and methods

2.1 Forecasting systems

ACCESS-S2 ([Wedd et al., 2022](#)) is the Bureau of Meteorology’s seasonal forecast system which became operational in October 2021, replacing the ACCESS-S1 system ([Hudson et al., 2017](#)). The model components of both ACCESS-S2 and ACCESS-S1 are identical with the same numbers of levels and resolution. They consist of the Global Atmosphere 6.0 (GA6) ([Williams et al., 2015; Waters et al., 2017](#)), the Unified Model’s Global Land 6.0 ([Best et al., 2011; Waters et al., 2017](#)), NEMO Global Ocean 5.0 ([Gurvan et al., 2013; Megann et al., 2014](#)) and Global Sea Ice 6.0 [CICE; [Rae et al. \(2015\)](#)]. The atmosphere has a N216 horizontal resolution (~60 km in the mid-latitudes) with 85 vertical levels. The land model uses the same horizontal grid as the atmosphere with four soil levels. The ocean component has a nominal horizontal resolution of 1/4° with 75 vertical levels. The sea-ice component, based on CICE version 4.1, has the same resolution as the ocean component and five sea-ice thickness categories as well as an open water category.

Both systems take atmospheric initial conditions derived from ERA-interim ([Dee et al., 2011](#)) for their hindcasts. The main difference between the hindcasts of the two systems are the ocean and sea-ice initial conditions.

ACCESS-S1’s ocean and sea-ice initial conditions come from the Met Office FOAM system, which uses a multivariate, incremental three-dimensional variational (3D-Var), first-guess-at-appropriate-time (FGAT) data assimilation scheme ([Waters et al., 2015](#)) and assimilates sea surface temperature (SST), sea surface height (SSH), in situ temperature and salinity profiles, and satellite observations of sea-ice concentration using the EUMETSAT OSISAF product described in the next section. The way sea-ice thickness is handled is that sea-ice concentration innovations are either added to the first ice category with a fixed thickness of 50cm or removed from the thinnest category first and from thicker categories if needed.

ACCESS-S2, on the other hand, is initialised from ocean conditions generated by the BoM weakly coupled ensemble data assimilation scheme described in [Wedd et al. \(2022\)](#). This scheme uses an optimal interpolation method and
85 assimilates temperature and salinity profiles from EN4 ([Good et al., 2013](#)). SSTs are nudged to Reynolds OISSTv2.1 ([Reynolds et al., 2007](#)) in areas where SSTs are over 0°C and Sea Surface Salinity is weakly nudged to the World Ocean Atlas 2013 climatology ([Zweng et al., 2013](#)).

Of most relevance for this work, sea-ice concentrations are not assimilated in ACCESS-S2. Assimilation cycles are performed daily. The coupled model runs for 24 hours initialised from the previous cycle. Then the restart file fields
90 of the ocean component are used as first guess in the data assimilation cycle and the innovations are used to build the next ocean initial conditions for the following cycle. The atmosphere fields from that daily integration are not used and instead the model atmosphere is initialised using ERA-Interim. The sea-ice initial conditions for the next cycle are the unaltered output of the previous daily integration. Then the cycle starts again and the coupled model runs for another 24 hours. During this integration the sea-ice component is affected by the ocean innovations and the
95 new atmosphere initial conditions via the coupler.

The ACCESS-S1 hindcast set is made up of nine members created by perturbing the atmospheric fields only with a random field perturbation ([Hudson et al., 2017](#)) and runs for 217 days for the period 1990–2012 initialised at the first of every month. The ACCESS-S2 hindcast set used in this study runs for the period 1981–2018. Ensemble members are created in the same manner as ACCESS-S1 members, however, due to computing cost limitations, only three
100 members per forecast initialisation date were run for 279 days. Bigger ensembles were generated by aggregating several three-member ensembles initialised on successive days ([Wedd et al., 2022](#)). Here, we build a nine-member time-lagged ensemble from three consecutive three-member forecasts initialised at the first of every month and the two previous days and run for 279 days. We analyse the ensemble mean hindcasts unless otherwise specified.

Anomalies for each hindcast set are taken with respect to their own climatology specific to each initialisation date
105 and forecast lead time, for the period 1990–2012. This serves as a first-order correction of model bias and drift. For monthly means, we define “0 lead time months” as the monthly mean forecast of the same month of initialisation.

Besides sea-ice concentration, we also analyse mean sea-ice thickness, which we compute as total sea-ice volume divided by total sea-ice area.

2.2 Verification datasets

110 For verification we use satellite-derived sea-ice concentration, which estimates the proportion of each grid area that is covered with ice. Datasets derived using different algorithms and satellite platforms, each have their own biases and uncertainties. Estimates of inter-product uncertainty of sea-ice extent (SIE, defined here as the total region of the Southern Ocean with at least 15% sea-ice cover) are of the order of 0.5 million km^2 ([Meier and Stewart, 2019](#)). As

will be shown below, this spread is minimal compared with the typical errors in the ACCESS-S2 and ACCESS-S1
115 forecasts, so the overall conclusions of this study are independent of the verification dataset used.

We use NOAA/NSIDC's Climate Data Record V4 [CDR; [Meier et al. \(2014\)](#)] as the primary sea-ice verification dataset. It takes the maximum value of the NASA Team ([Cavalieri et al., 1984](#)) and NASA Bootstrap ([Comiso, 2023](#)) sea-ice concentration products to reduce their low concentration bias ([Meier et al., 2014, 2021](#)). Both source algorithms use data from the Scanning Multichannel Microwave Radiometer (SMMR) on the Nimbus-7 satellite
120 and from the Special Sensor Microwave/Imager (SSM/I) sensors on the Defense Meteorological Satellite Program's (DMSP) -F8, -F11, and -F13 satellites. The data have a spatial resolution of 25 by 25 km and daily from November 1978 onwards.

The European Organisation for the Exploitation of Meteorological Satellites (EUMETSAT) Ocean and Sea Ice Satellite Application Facility [OSI; [EUMETSAT Ocean and Sea Ice Satellite Application Facility](#)] based on the SSMIS
125 sensor is another satellite-derived sea-ice concentration product. It is based on mostly the same sensors as the NOAA CDR but computed independently using different algorithms. Figures prepared with this dataset are provided in the appendix and do not differ significantly from the ones prepared using CDR.

2.3 Error measures

For evaluation purposes, we use a series of measures. Sea-ice extent is defined as the area of the ocean at least 15%
130 covered by sea-ice. This threshold is motivated by the limitations in satellite retrieval, which is increasingly unreliable for lower sea-ice concentrations ([Cavalieri et al., 1991](#)). We evaluate sea-ice extent anomaly hindcasts by their Root Mean Squared Error (RMSE) and correlation coefficient. The hindcast ensemble mean sea-ice extent is defined as the sea-ice extent of the ensemble mean hindcast.

Pan-Antarctic (net) sea-ice extent serves as a hemispheric measure of the amount of sea ice, but it does not take into
135 account the spatial distribution. A model could have a relatively accurate extent of the net ice but with different regional distributions. To account for location errors, we computed the RMSE of grid-point sea-ice concentration anomalies.

We compute RMSE as the square root of the area-averaged squared differences between grid-point forecasted and observed sea-ice concentration anomalies. We compute a pan-Antarctic RMSE by averaging over the whole
140 NOAA/NSIDC CDRV4 Southern Hemisphere domain, and also a zonally-varying RMSE computed over 15 longitude slices 24° wide around Antarctica.

All error measures were computed on the NOAA/NSIDC CDRV4 domain grid, to which model output was bilinearly interpolated. Note that the ACCESS CICE model grid has resolution between two and three times higher than NOAA/NSIDC CDRV4.

145 Forecast errors are also compared with hypothetical forecasts based on the persistence of anomalies and on climatology. The persistence forecast is generated by extending the observed sea-ice concentration anomalies the day of the forecast initialisation and comparing it with the actual anomalies observed. The climatological forecast error is computed as the standard deviation of daily anomalies.

150 As a measure of forecast improvement over the hypothetical forecast, we use the skill score ([Murphy and Daan, 1985](#)), defined as

$$S = 1 - \frac{RMSE_f}{RMSE_r}$$

Where $RMSE_f$ is the RMSE of the forecast, $RMSE_r$ is the RMSE of the reference forecast. Negative skill score indicates that the forecast is worse than the reference forecast while positive values indicate an improvement. A perfect forecast would have zero RMSE and thus a skill score of 1.

155 Furthermore, we also compute sea-ice concentration bias, defined as the mean difference between the forecast and observations.

2.4 Computational procedures

We performed all analyses in this paper using the R programming language ([R Core Team, 2020](#)), using data.table ([Dowle and Srinivasan, 2020](#)) and metR ([Campitelli, 2020](#)) packages. Significant processing was performed using the 160 CDO command line operators ([Schulzweida, 2023](#)). All graphics are made using ggplot2 ([Wickham, 2009](#)). The paper was rendered using knitr and Quarto ([Xie, 2015; Allaire et al., 2022](#)).

3 Results and discussion

3.1 Bias

Figure 1 (Figure A1 for OSI) shows mean sea-ice extent of the ACCESS-S1 and ACCESS-S2 hindcasts (row a) 165 and their differences from mean sea-ice extent of NOAA/NSIDC CDRV4 (row b). Mean extent at the first of every month is indicated with circles for the initial conditions and with triangles for the longest lead time possible for each model (between 274 and 277 days for ACCESS-S2 and between 213 and 216 days for ACCESS-S1). At this long lead time, information of the initial conditions is essentially lost and the forecast reverts close to each model's preferred equilibrium state.

170 ACCESS-S2 initial conditions (circles in Fig. 1 column 2) show an overall negative bias, especially in the late summer-early autumn, while ACCESS-S1 initial conditions (circles in Fig. 1 column 1) are very close to observations,

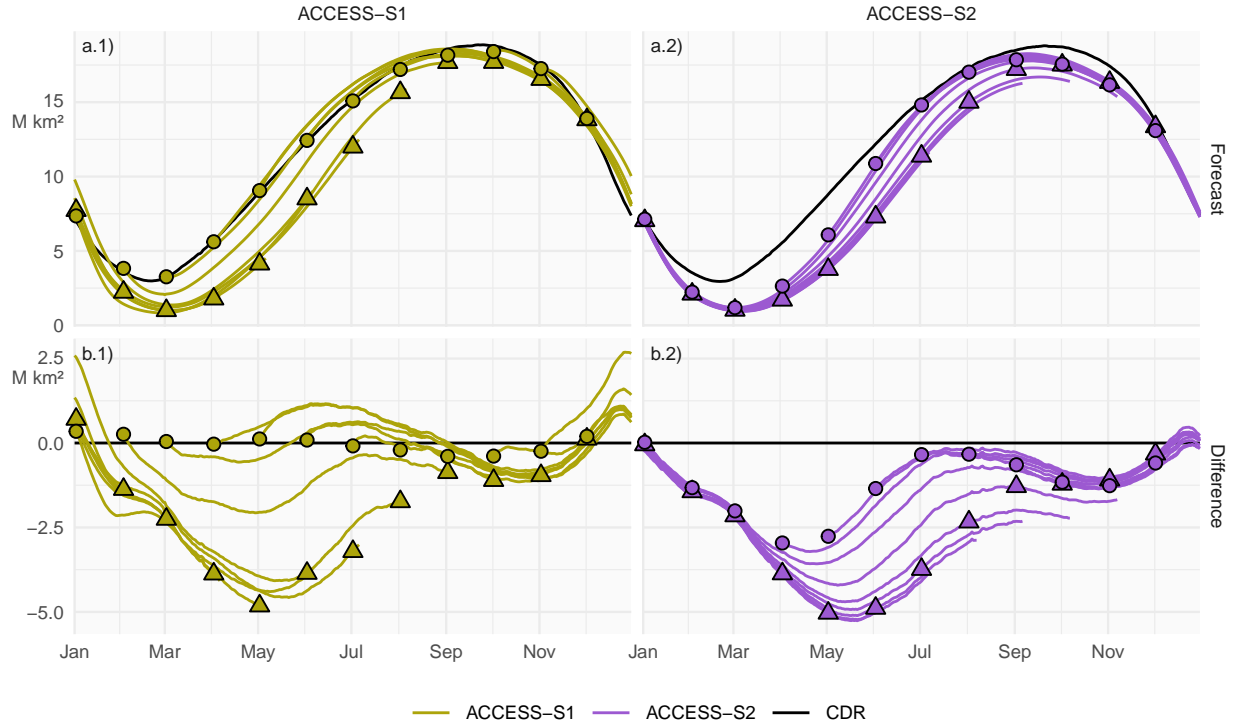


Figure 1. Row a: Pan-Antarctic daily mean sea-ice extent for all hindcasts initialised on the first of each calendar month for ACCESS-S1 (column 1; green) and ACCESS-S2 (column 2; purple). Observed mean sea-ice extent in each corresponding hindcast period is shown in black. Row b: Mean differences between the forecast and the observed values. Circles represent the initial conditions at the start of forecasts (i.e., the first of every month), and triangles represent the mean values at the lead time corresponding to the maximum lead time in S1 (between 213 and 216 days, depending on the month)

as expected from the assimilation of sea-ice observations to produce the initial conditions of ACCESS-S1. Both systems' equilibrium states (triangles) show negative biases of sea-ice extent, particularly in the growth phase of late-autumn and winter months. This is due primarily to the melt season being longer than in observations and with
 175 faster melt between January and March and the growing seasons being shorter with slower growth during March and April. This is then followed by faster growth between May and July (Figure 2 and Figure A2). Many sea-ice models exhibit this systematic underestimation during the sea-ice minimum and early freezing season (Massonnet et al., 2023), which could indicate problems in the representation of thermodynamics in the model (Zampieri et al., 2019). It is also not surprising that both forecasting systems converge to a similar equilibrium state because they share the
 180 same model formulation.

The difference between the initial conditions (circles) and the model equilibrium state (triangles) can be mostly attributed to the effect of data assimilation, which in ACCESS-S2 is due solely to the coupling of sea-ice with the

atmosphere and the ocean. From April to September, in ACCESS-S2 circles are closer to observations than the triangles are, indicating that the information from the ocean and atmosphere data assimilation is affecting sea ice
185 and improving the initial conditions. During these months, ACCESS-S1 can overestimate the sea-ice extent at short lead time. For the rest of the year circles are overlaid with triangles in ACCESS-S2, indicating that the ocean and atmosphere data assimilation is not affecting sea ice and that this component of the model is virtually free-running.

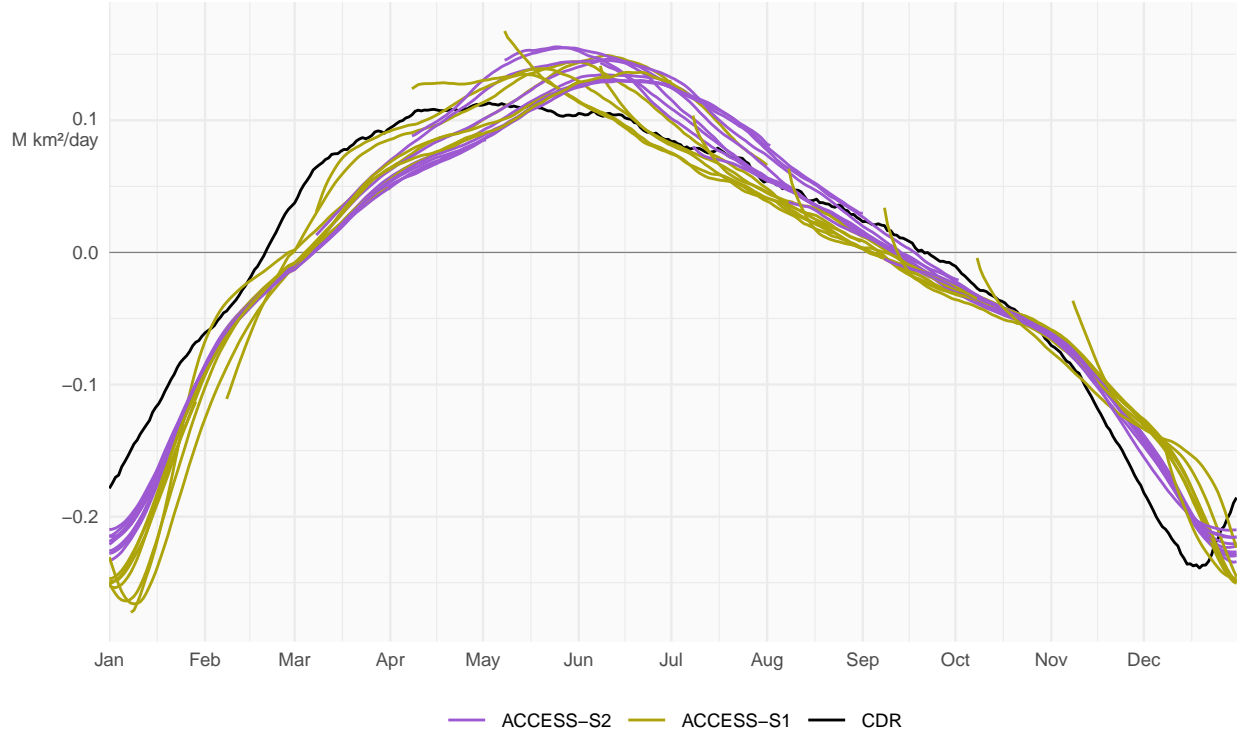


Figure 2. Mean daily sea-ice extent growth ($10^6 \text{ km}^2/\text{day}$) in ACCESS-S1 (green) and ACCESS-S2 (purple) hindcasts and observations (black), computed as the mean daily differences in sea-ice extent between each date and the next for each forecast month. Values are smoothed with a 11-day running mean.

To further understand the bias in ACCESS-S2, Figure 3 (Figure A3) shows spatial patterns of the differences of monthly mean sea-ice concentrations between NOAA/NSIDC CDRV4 and ACCESS-S2 hindcasts at the shortest
190 monthly lead time. From October to May, the model underestimates sea-ice concentrations in most regions except for the inner Weddell Sea in April and May, where sea-ice concentrations saturate to 1 both in the observations and forecasts. In winter, the differences are limited to a narrow band around the sea-ice edge with slight positive biases in the African sector of East Antarctica and negative biases around the Indian Ocean sector which partially compensate, resulting in the near-zero extent bias seen in those months (Figure 1).

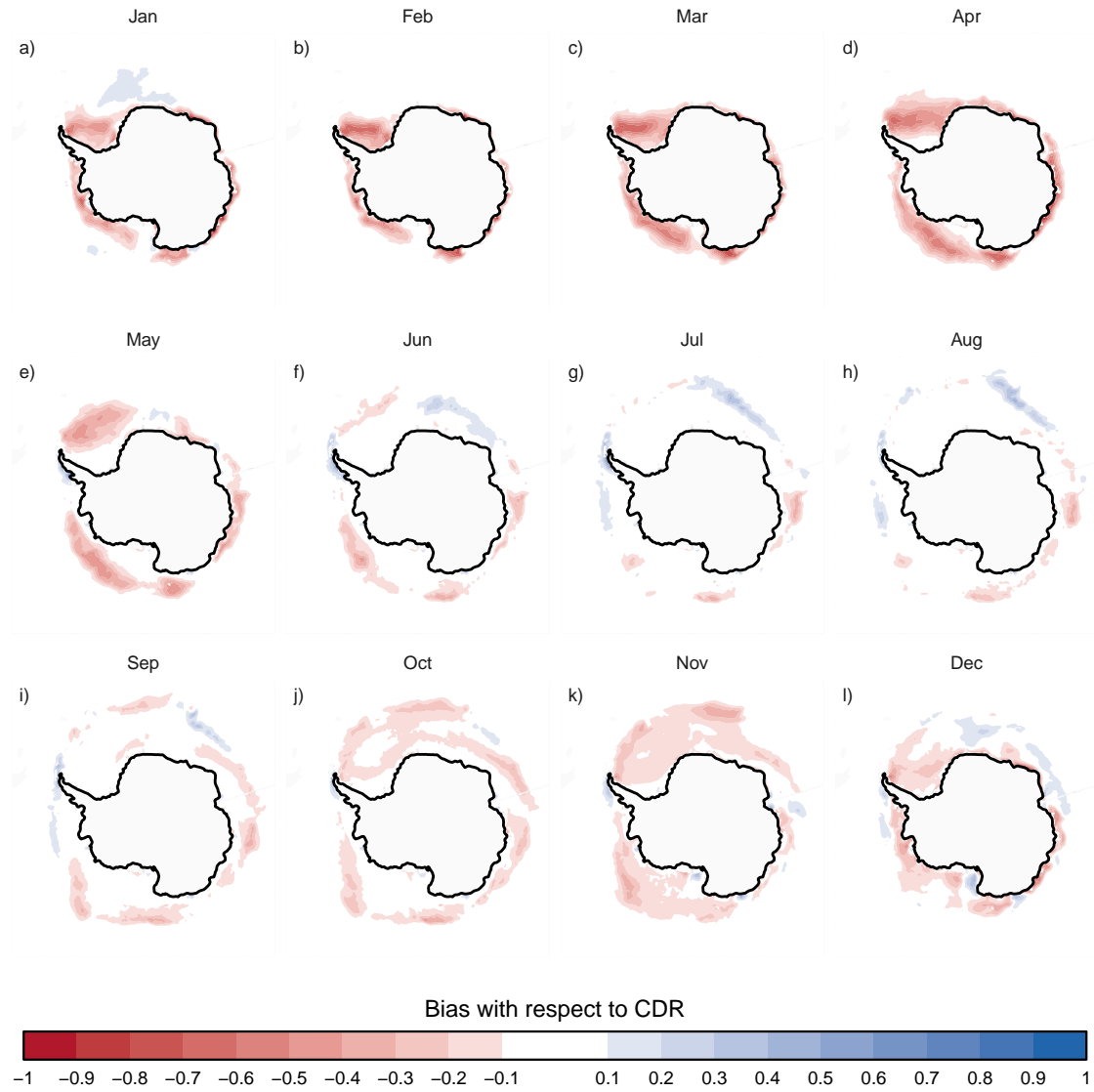


Figure 3. expression(glue::glue("Ensemble mean difference between monthly sea-ice concentration of ACCESS-S2 ensemble mean forecast at 0-month lead time (monthly mean values forecasted from the forecast initialised at the first of the month) and observations (CDR)."))

195 ACCESS-S1 has a comparatively smaller overall bias (Figure 4 and Figure A4). The largest values are found between April and June, when the faster growth results in large positive bias along the sea-ice edge, and in January, when the faster melt leads to large negative bias in the Weddell and Amundsen Seas.

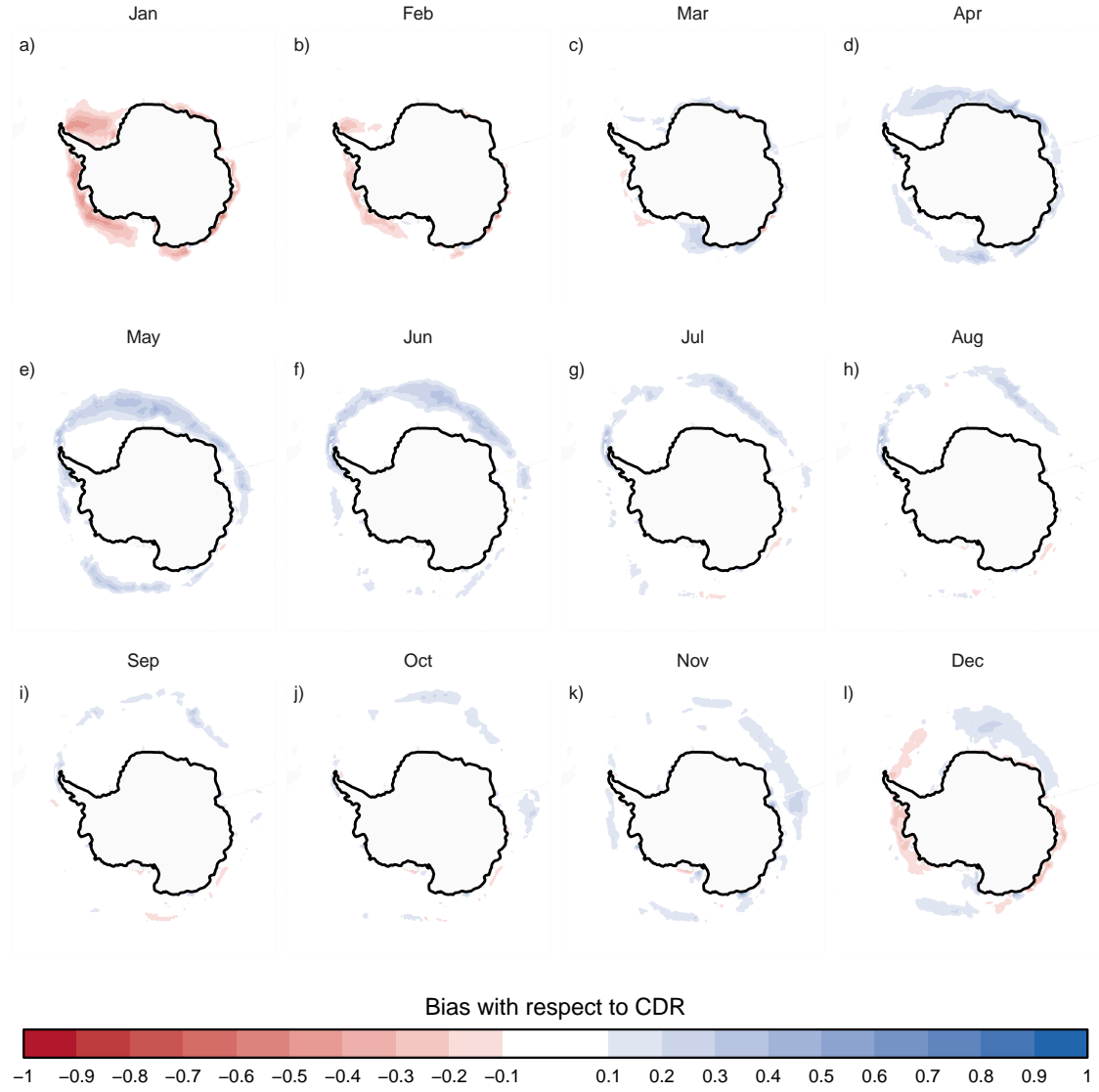


Figure 4. Same as Figure 3 but for ACCESS-S1.

3.2 RMSE

Figure 5 (Figure A5) shows monthly sea-ice extent anomalies forecasted at selected lead times. Compared with
200 ACCESS-S1, ACCESS-S2 anomaly forecasts are relatively poor (large RMSE) even for the first month (lead time 0), whereas ACCESS-S1 forecasts stay relatively skilful even at a lead time of three months. ACCESS-S2 shows much

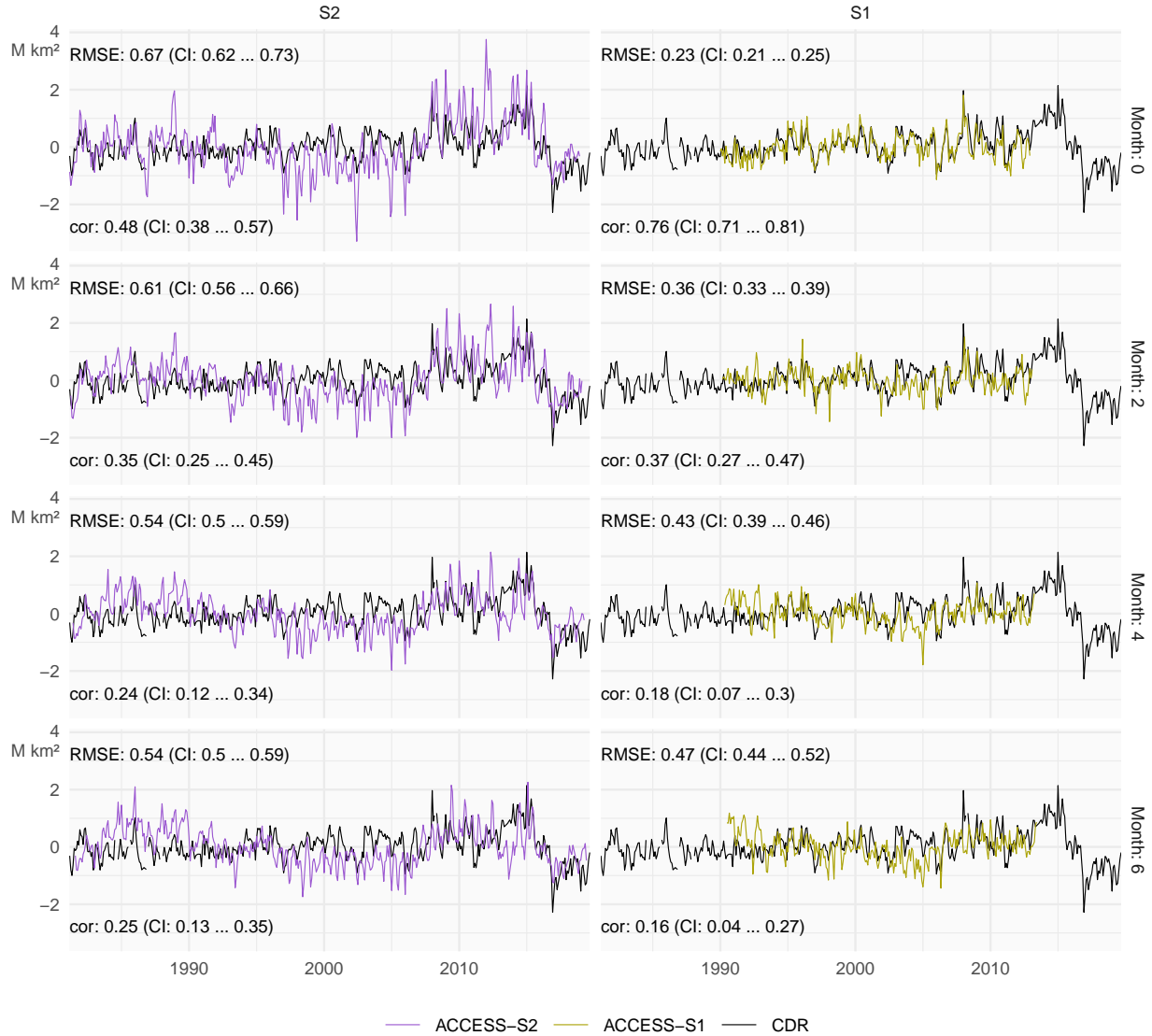


Figure 5. Monthly mean sea-ice extent anomalies of the observations (black) and forecasts from ACCESS-S1 (right column; purple) and ACCESS-S2 (left column; green) at lead times of 0, 2, 4, and 6 months. The RMSE and correlation with their respective 95% confidence interval during the overlapping period of ACCESS-S1 and ACCESS-S2 hindcasts (1990–2013) are shown on the top left and bottom left of each panel respectively

larger interannual variability than observations, with dramatic lows between 1995 and 2007, and highs between 2007 and 2015.

Unexpectedly, for ACCESS-S2, RMSE improves with lead time, even though the correlation degrades with lead time. This effect is seen in all months except from July to September Figure A6. This is puzzling behaviour that goes contrary to what is usually seen in prediction models. The explanation seems to be the mentioned increased interannual variability. Figure 6 (Figure A7) shows the interannual standard deviation of monthly sea-ice extent of the forecasts as a function of lead time compared with observations. ACCESS-S1 standard deviation lies within the observed standard deviation regardless of lead time, while ACCESS-S2 standard deviation is more than twice that of observations at zero lead time and only approaches the observed value at nine month lead time for most months.

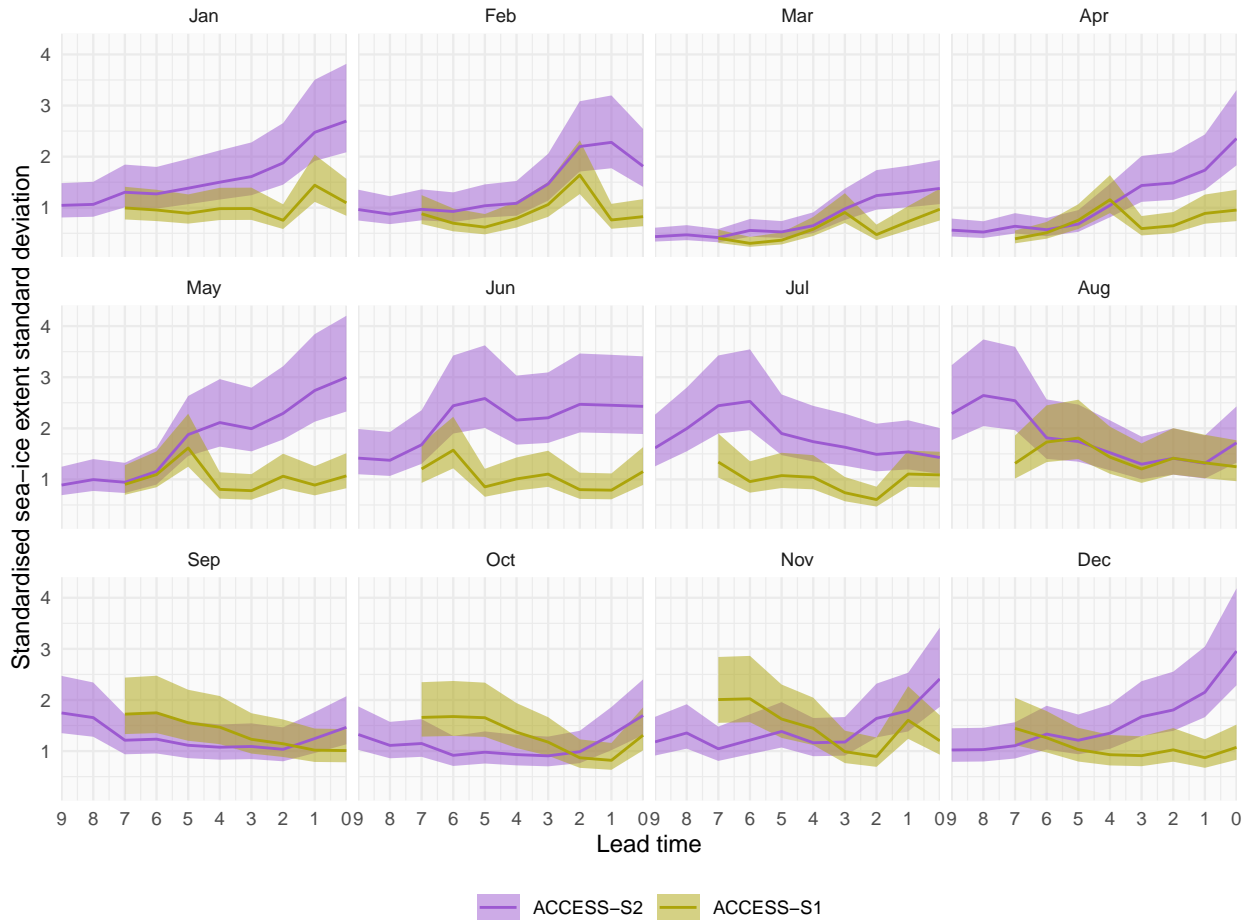


Figure 6. Interannual standard deviation with 95% confidence interval of monthly mean sea-ice extent forecasted for each month. We standardise the standard deviation by that month's sea-ice extent observation standard deviation. ACCESS-S1 and ACCESS-S2 at different lead times. Each panel indicates the target month. Note the reverse horizontal axis.

ACCESS-S2 forecasts of sea-ice extent anomalies seem to align moderately well with observations (leading to moderately high correlation) but their magnitude is overestimated (leading to large errors). This could be caused by ACCESS-S2 sea ice being much more sensitive to atmospheric and oceanic forcing, perhaps due to lower thickness.

As an example, Figure 7 shows sea-ice concentration anomalies (top row) and sea-ice thickness and the difference 215 between the two models (bottom row) for 2 May 2008 initialised one day prior; being that close to initialisation date, these are very approximately the initial conditions. ACCESS-S1 sea-ice concentrations anomalies are very close to observations as expected from the system assimilating these data. ACCESS-S2 sea-ice concentration anomalies, which are not assimilated, are not as close, but the large-scale pattern is aligned with observations. The system 220 simulates large positive anomalies in the Weddell and Ross Seas and slight negative anomalies in the Amundsen and Bellingshausen Seas. The fact that ACCESS-S2 can simulate this pattern without assimilating sea-ice data suggests that atmospheric and oceanic forcing were the dominant drivers. However, the magnitude of the sea-ice anomalies is too big. It is plausible that this is due to the thinner ice simulated by ACCESS-S2 (bottom row).

Extending beyond the one case in Figure 7, Figure 8 shows monthly mean sea-ice thickness as a function of lead time 225 for ACCESS-S1 and ACCESS-S2. Supporting the idea that thinner ice is what causes the increased extent variability in ACCESS-S2, this system simulates thinner sea-ice compared to ACCESS-S1 overall at almost all lead times and in all months except for summer at short lead times (Dec-Jan, 0-1 months; Feb-Mar, 0-2 months). However, in both systems, forecasted sea-ice is thicker at shorter lead times and then decreases, particularly in the summer months. If thinner ice were a sufficient cause of increased variability, then we would expect variability to increase with lead time in both forecasting systems.

230 The fact that ACCESS-S1 and ACCESS-S2 share the same model configuration and that the increased variability is more extreme at short lead times (Fig. 6) suggests that the data assimilation procedure is partly responsible. It is possible that sea-ice in the ACCESS-S2 system is left in an unbalanced state after assimilating atmospheric and oceanic data but not sea-ice data, leading to large responses that are amplified by the thin ice in the initial states which then subside at longer lead times when the model is balanced.

235 To assess ACCESS-S2 forecasts in more detail, we compute error measures for all hindcasts started on the 1st of every month. Figure 9 (Figure A8) shows the mean RMSE of sea-ice concentration anomalies for ACCESS-S1 and ACCESS-S2 hindcasts compared against persistence and climatological forecasts used as a benchmark. Due to errors in the initial conditions, it is expected that persistence forecasts would be better than the model forecasts at very short lead times, but that the persistence forecast errors would grow faster and may eventually surpass the model 240 forecast errors. The black line shows that the persistence forecast error indeed grows rapidly and reaches its maximum in about 30 days for most months except for February, when it grows much slower. The ACCESS-S1 forecast errors grow slower than persistence forecast errors and remain lower after less than 10 days on average. The ACCESS-S2 forecast error starts high in all months and is lower than the persistence forecast error after more than 15 days in most months except for forecast initialised in February, when it takes 80 days.

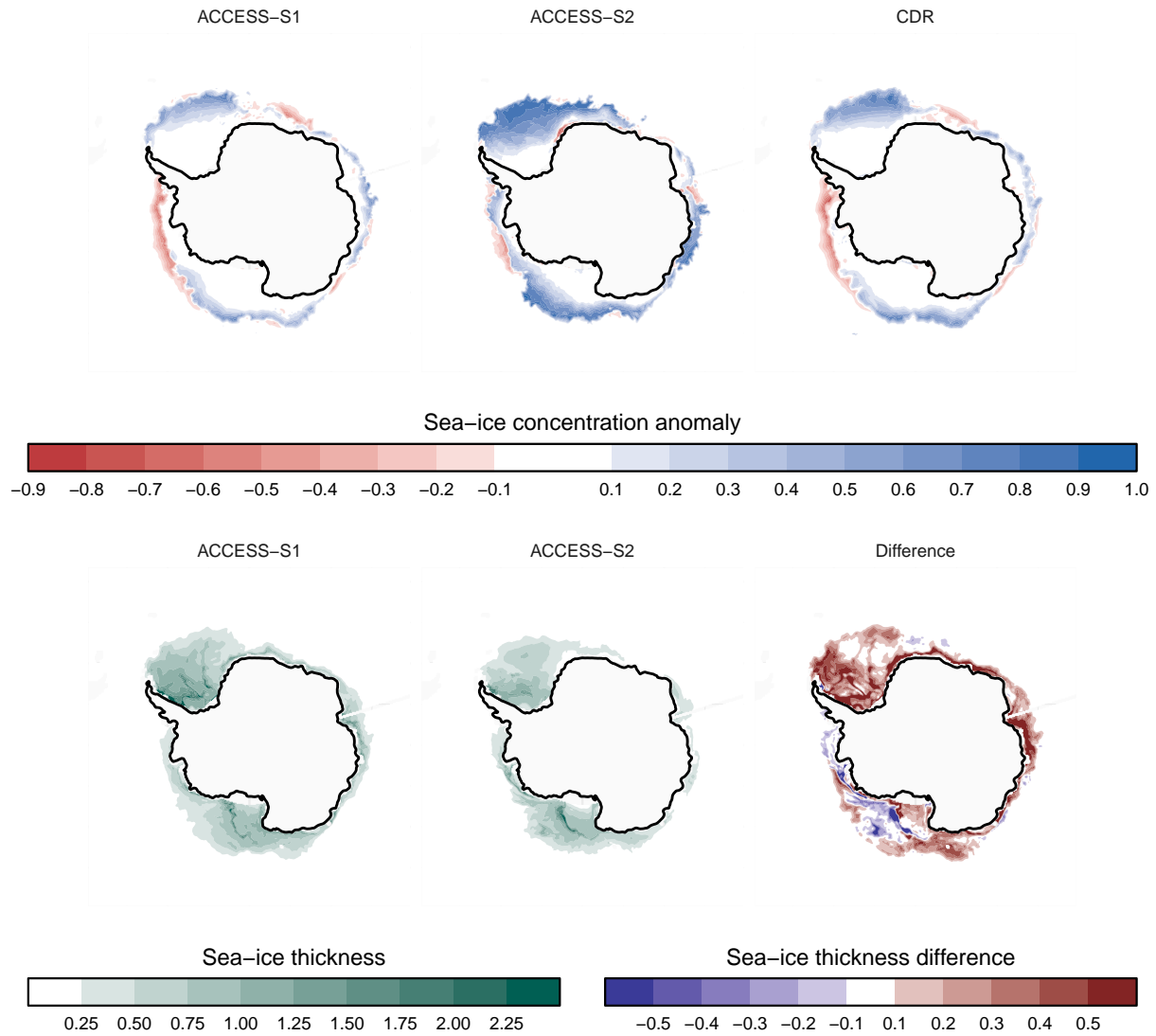


Figure 7. ACCESS-S1 and ACCESS-S2 hindcasts for 2 May 2008 at one day lead time. Top row shows sea-ice concentration anomalies forecasted by each system and the observations. Bottom row shows forecasted sea-ice thickness and the difference between ACCESS-S1 and ACCESS-S2.

245 At longer lead times, it is more appropriate to compare errors with the climatological forecast error. The lead time at which ACCESS-S1 forecast error is higher than the climatological forecast error varies between more than 60 and less than 20 days depending on forecast initialisation month with the minimum in June. ACCESS-S2 forecasts never have lower error than climatology, on the other hand, except marginally in October forecasts.

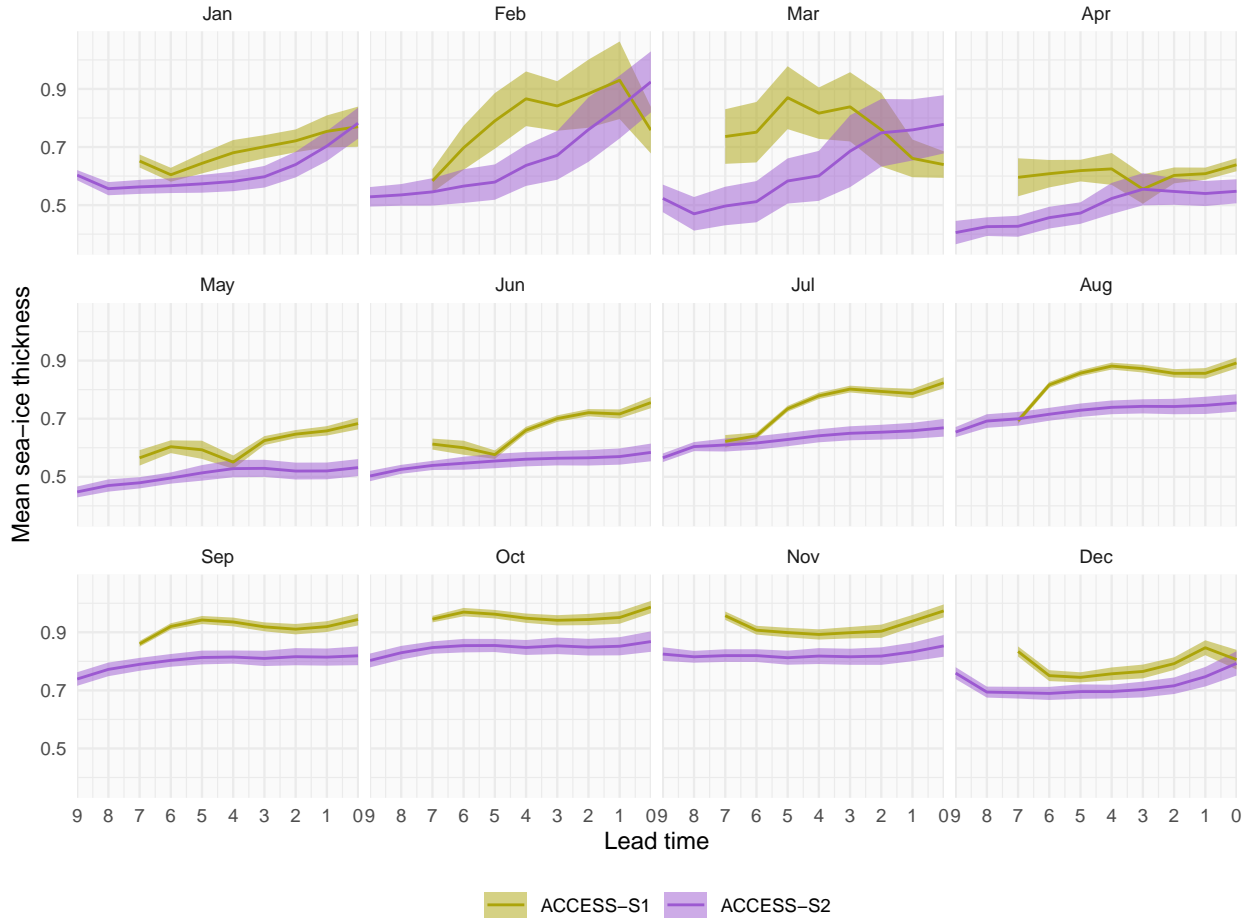


Figure 8. Mean and 95% interval of monthly mean sea-ice thickness for ACCESS-S1 and ACCESS-S2 at different lead times. Each panel indicates the target month. Note the reverse horizontal axis.

Figure 10 (Figure A9) summarises the lead time window in which each hindcast is better than both the persistence forecast and the climatological forecast as a function of forecast month. ACCESS-S1 forecasts have a wider lead time window in the summer than the other seasons and is not better than both benchmarks at forecasting June sea-ice concentration anomalies. Forecasts initialised between May and July are particularly poor, and June cannot be forecasted better than the benchmarks. This is consistent with the mid-winter loss of predictability observed by Libera et al. (2022), who attributed it to deep warm water entraining into the mixed layer.

To analyse the spatial distribution of the model error, we computed the RMSE of zonal mean sea-ice concentration anomalies on 15 slices of 24° longitude span for each forecasting system. We control for some areas being naturally easier to forecast than others by computing the RMSE skill score with the climatological forecast RMSE as reference.

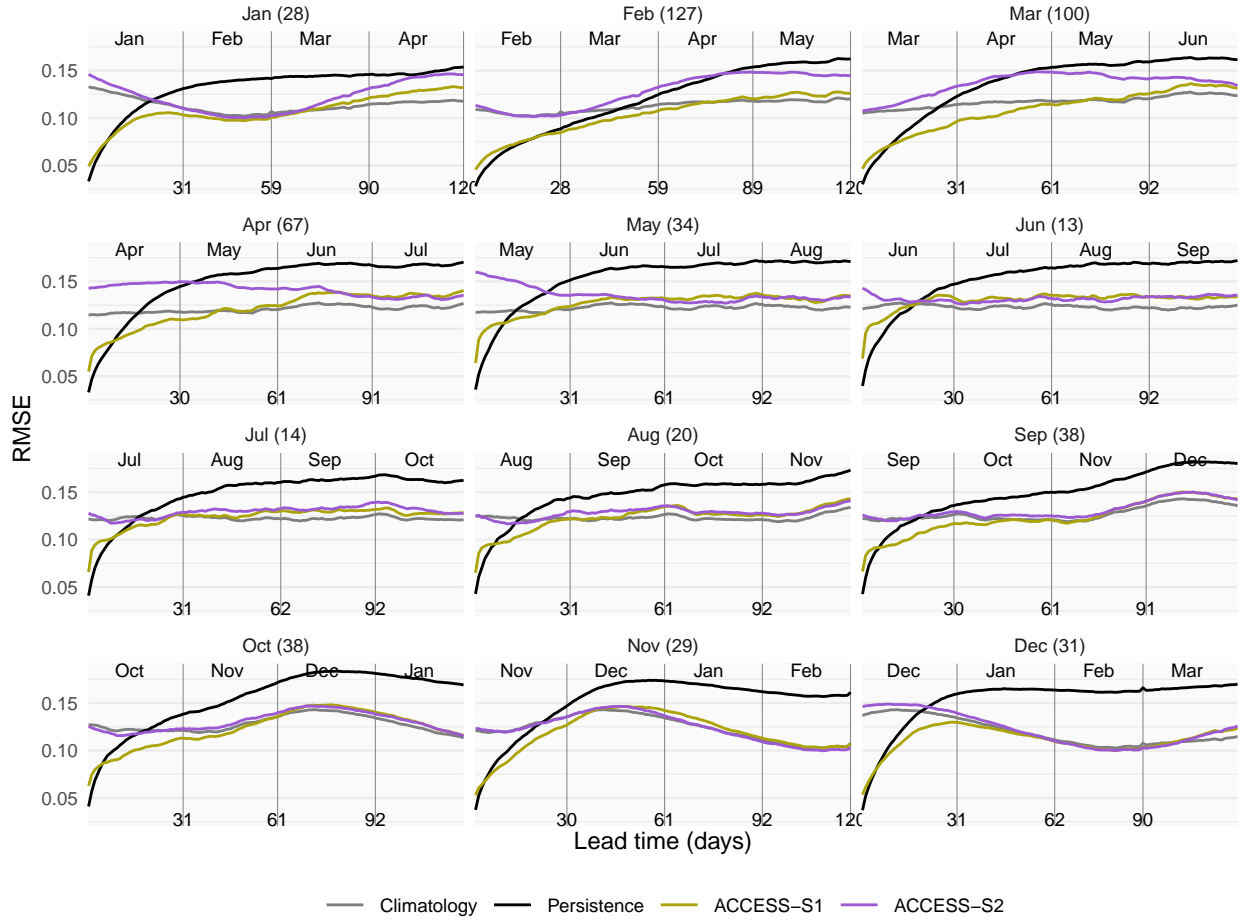


Figure 9. Mean RMSE of sea-ice concentration anomalies as a function of forecast lead time for all forecasts initialised on the first of each month compared with a reference forecast of persistence of anomalies (black) and climatology (gray). Only the first 120 days are shown. In parentheses, the shortest time at which ACCESS-S1 and ACCESS-S2 mean RMSE is not statistically different at the 99% confidence level.

For ACCESS-S1 forecasts (Figure 11 and Figure A10), skill tends to be lower off the coast of Eastern Antarctica even at short lead times; for instance, the skill score for forecasts initialised in May and June are negative between 0° and 260 120°E even at almost zero lead time. This mirrors Libera et al. (2022) findings of a “winter predictability barrier”, although they focus on the Weddell Sea and here we show that the effect seems to be stronger more to the east. In West Antarctica there is a hint of easterly-propagating skill in forecasts initialised in February and March. This is consistent with Holland et al. (2013) findings that memory of sea-ice anomalies are stored in ocean heat content anomalies that are transported east by the Antarctic Circumpolar Current.

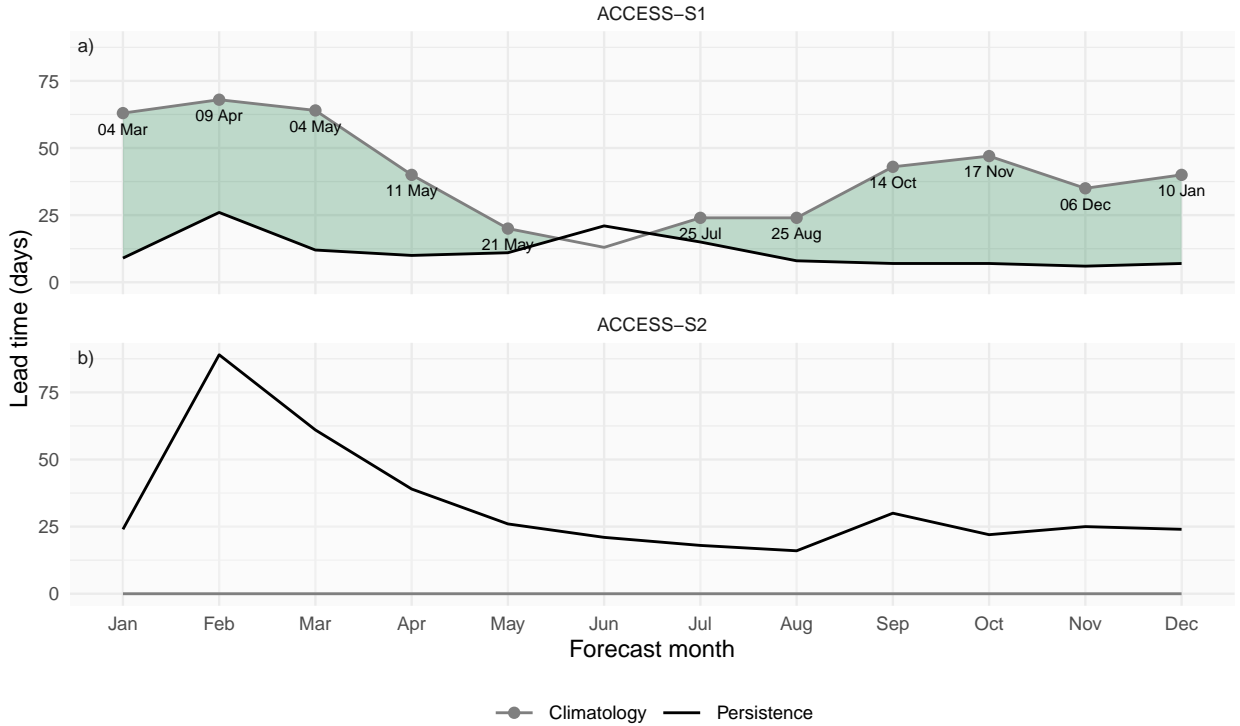


Figure 10. Minimum lead time at which each forecast's mean RMSE becomes larger than the lower bound of the 95% confidence interval of persistence forecast RMSE (black lines) and maximum lead time at which each forecast's mean RMSE remains lower than the lower bound of the 95% confidence interval of climatological forecast RMSE (gray lines). Green shading indicates the window where forecasts outperform both persistence (lead times longer than black line) and climatology (lead times shorter than gray line). Text labels show the date corresponding to the maximum lead time at which each forecast outperforms climatology.

265 ACCESS-S2 forecasts (Figure 12 and Figure A11) also have lower skill over East Antarctica. From July to December even though the pan-Antarctic average skill is negative at all lead times (Fig. 10), it is positive for up to a month in West Antarctica. Since oceanic and atmospheric forcing is the only source of information, this suggests that sea-ice in this region is particularly sensitive to oceanic and atmospheric forcing and suggests a role of the Pacific-South American mode and the Amundsen Sea Low to shape sea-ice concentration anomalies. The fact that this is evident
 270 in the months in which El Niño–Southern Oscillation teleconnections are more important for atmospheric circulation also suggests the influence of tropical Pacific variability. February and March are the only two months that can be forecasted with marginally positive skill in large regions.

Finally, Figure 13 (Figure A12) shows the difference in skill between ACCESS-S1 and ACCESS-S2. Large differences in skill indicate areas and months that are most affected by the data assimilation present in ACCESS-S1. Between

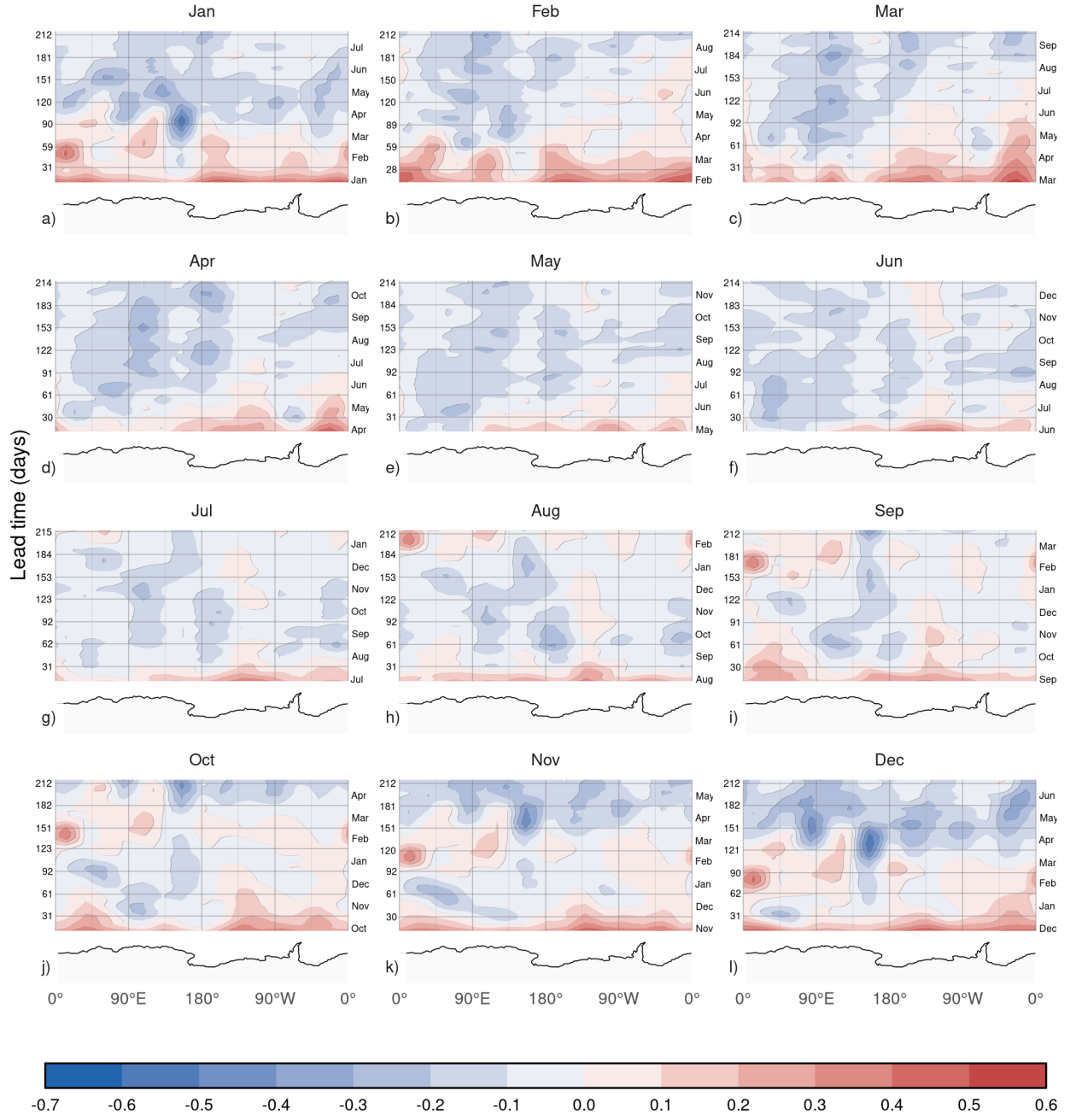


Figure 11. MSE skill score of ACCESS-S1 forecasts with climatological forecast as reference computed on 15 meridional slices 24° wide as a function of lead time and longitude. Antarctica's coastline is shown at the bottom of each panel for reference. Values were smoothed with an 11-day running mean to improve readability.

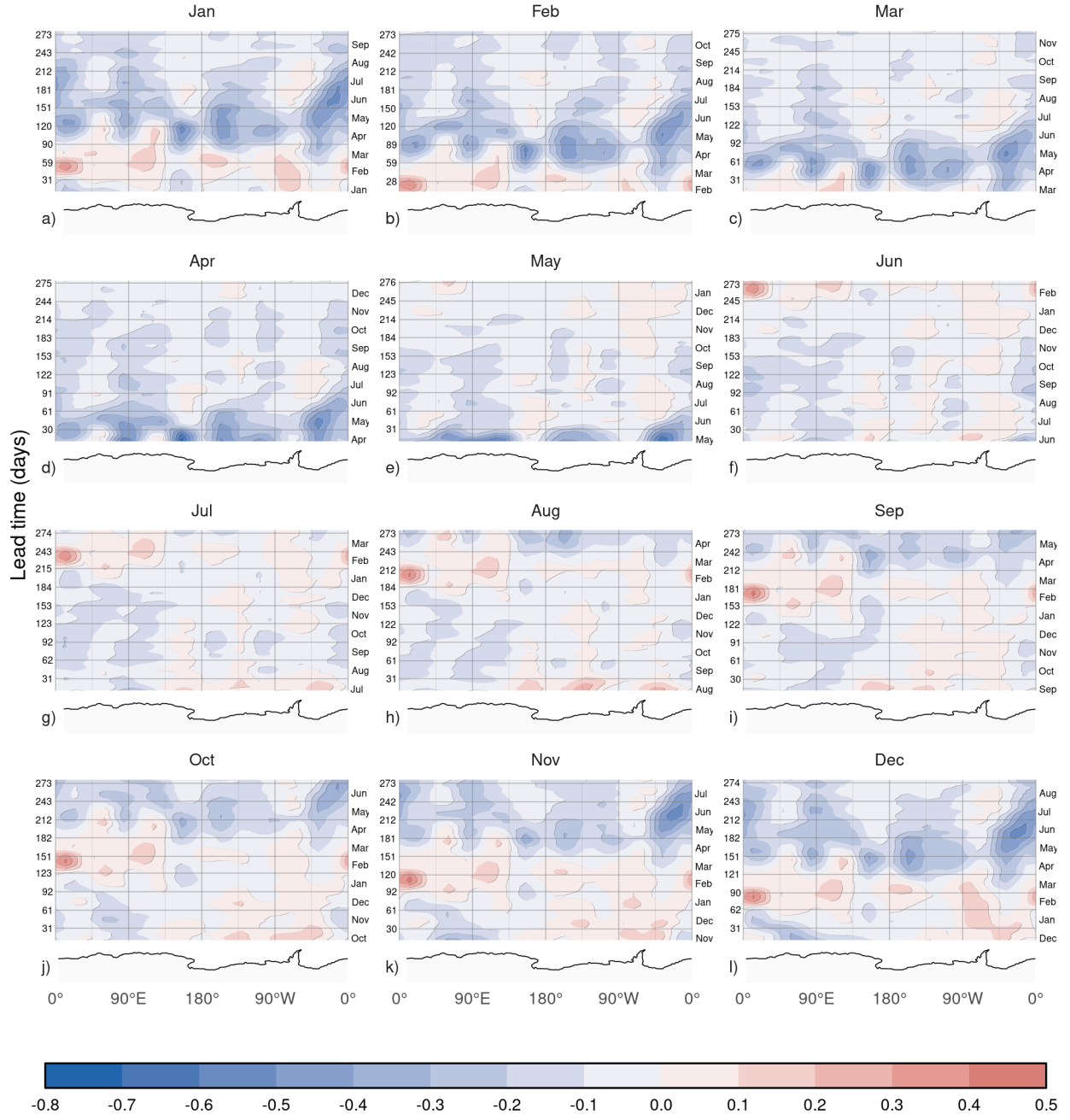


Figure 12. Same as Figure 11 but for ACCESS-S2.

275 January and March, which are the months in which ACCESS-S1 is the most skilful (Figure 10), most of the

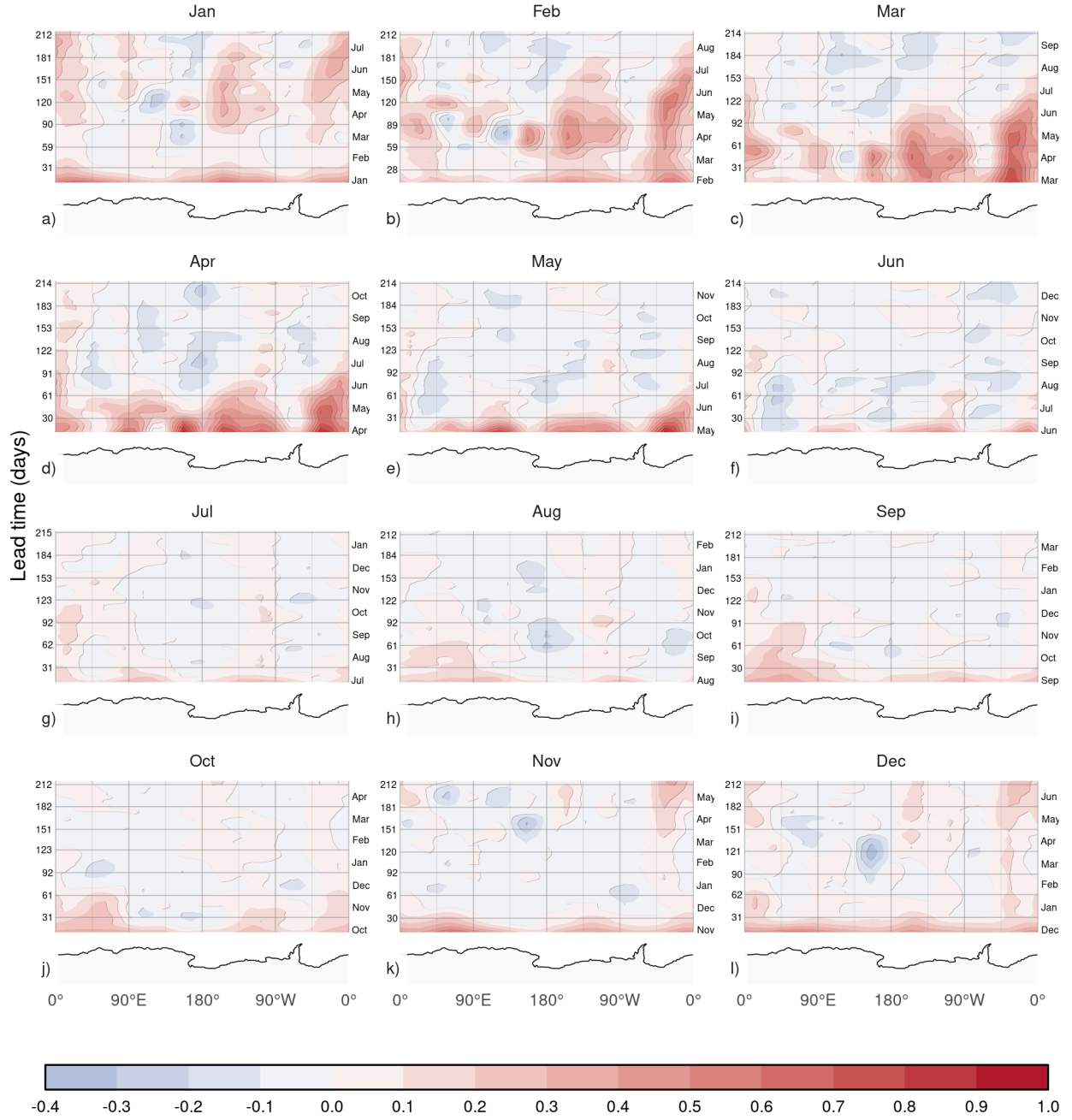


Figure 13. Same as Figure 11 but for the difference between ACCESS-S1 and ACCESS-S2.

improvement compared with ACCESS-S2 is present in the Ross and Weddell Sea. In April and May, the improvement seems more homogeneous.

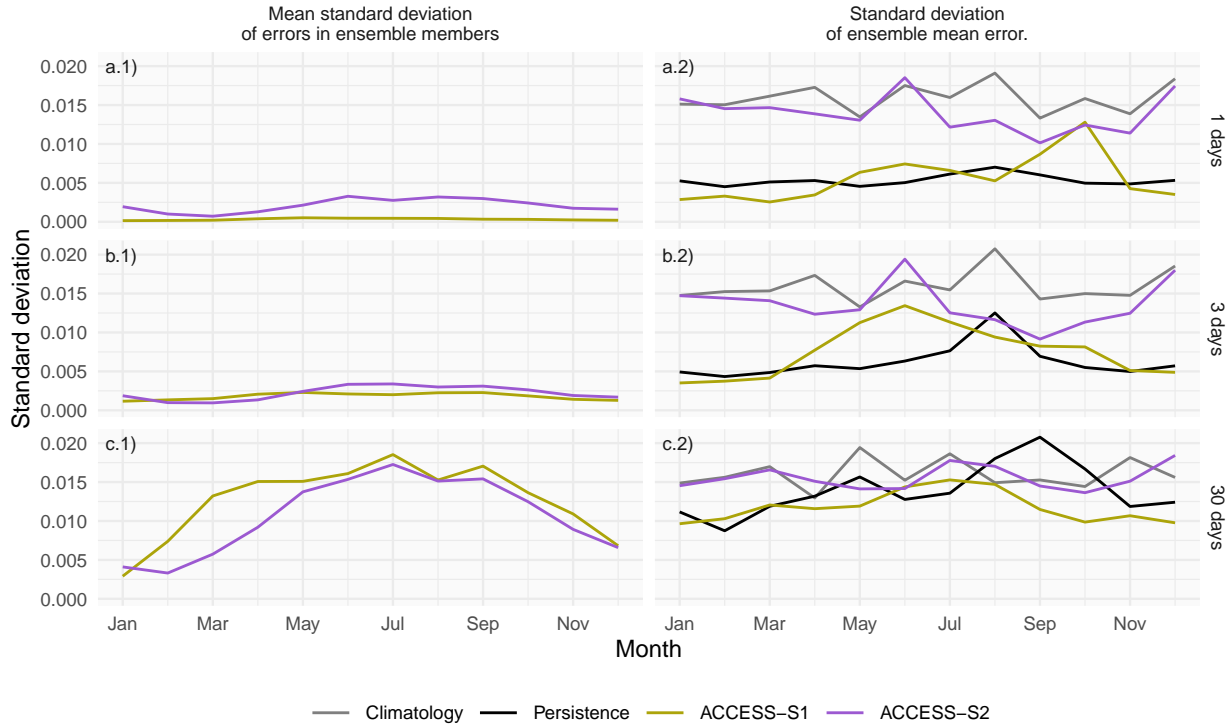


Figure 14. Decomposition of forecast error spread at 1, 5 and 30 days lead time for ACCESS-S1 and ACCESS-S2 hindcasts across initialization months. The left column shows the mean standard deviation of RMSE errors across ensemble members, while the right column shows the standard deviation of the ensemble mean RMSE error and the spread of the persistence and climatology forecasts errors.

In Figure 9 the mean error was shown. Figure 14 (Figure A13) column 1 shows the mean standard deviation of errors among ensemble members at various lead times. At one day lead time (Fig. 14 a.1) ACCESS-S2 has a slightly larger spread than ACCESS-S1 due to the way that ensemble members are generated. ACCESS-S1 ensemble members are generated by adding random field perturbations to the atmosphere only, which then are transferred to the other components via the coupled simulation (Hudson et al., 2017). With this scheme, ensemble members are all but guaranteed to be underdispersed in the ocean and sea-ice components. The time-lag ensemble used for ACCESS-S2 ensures greater spread. This difference is gone after about just two days, and both systems have a comparable spread in ensemble member error afterwards (Fig. 14 b1 and c1).

Figure 14 column 2, on the other hand, shows the standard deviation of ensemble mean error of each hindcast and the persistence forecast. At one day lead time, ACCESS-S2 ensemble mean error standard deviation is much larger than ACCESS-S1's, which in turn is comparable to the persistence forecast error standard deviation. At longer lead times, the spread of ACCESS-S1 and persistence forecast standard deviation increases to eventually be comparable

290 to ACCESS-S2 and the standard deviation in climatological forecast errors. ACCESS-S2 error standard deviation is fairly independent of lead time and similar to the climatological forecast error standard deviation at all lead times.

3.3 Conclusions

Sea-ice forecasts from the ACCESS-S2 system show a significant low extent bias, particularly during late summer and early autumn. This bias is attributed to a faster and longer melt season between January and March, and 295 slower growth between March and April. This underestimation during the minimum and early freezing season is a common issue in many subseasonal-to-seasonal (S2S) systems, suggesting potential problems either with the model's thermodynamic representation or with short wave radiation forcing, as shown in other climate models ([Zampieri et al., 2019](#); [Roach et al., 2020](#)). Even though ACCESS-S2 shares the same model components as ACCESS-S1, the latter does not suffer from this bias, indicating that assimilating sea-ice concentrations successfully corrects for the 300 negative bias that exists in the free-running model.

Ensemble spread grows quickly even when perturbations are only implemented in the atmosphere component (in ACCESS-S1), indicating that sea ice is indeed responding quickly to atmospheric perturbations. However, our analysis suggests that the atmosphere and ocean data assimilation implemented in ACCESS-S2 is only effectively influencing sea-ice initial conditions from June to October, while the rest of the year, the sea-ice component runs virtually 305 free, reverting to its biased equilibrium state. [Zhou and Alves \(2022\)](#) had previously evaluated sea-ice forecasts in ACCESS-S2 and also highlighted the poor performance of this forecasting system attributed to the lack of good initial conditions.

Analysis of the error spread shows that ACCESS-S2 initial conditions from December to May not only have large 310 errors, but that the initial error spread is very large compared with ACCESS-S1. This spread is not due to the perturbation scheme, since the mean error variance for individual forecasts is low and comparable with ACCESS-S1. Instead, it is due to large variance of the mean error of individual forecasts, which is comparable to the climatology spread. This is further evidence that individual initial conditions are not being affected by the data assimilation scheme.

Although ACCESS-S1 only assimilates sea-ice concentration, it is clear that sea-ice thickness is also affected through 315 the assimilation process. ACCESS-S1 simulates significantly thicker ice than ACCESS-S2 and in both systems sea-ice is thicker at shorter lead times than at longer lead times. Both the explicit data assimilation in ACCESS-S2 and the effects of atmospheric and oceanic data assimilation in ACCESS-S1 might be nudging simulated sea ice to be thicker than the model equilibrium state. We suggest that the thinner sea ice in ACCESS-S2 contributes to the large sea-ice extent variance, but other mechanisms, such as unbalanced initial conditions might also be important.

320 Given that ACCESS-S2 sea-ice extent is not directly initialised by sea-ice observations, comparing its forecasts with those of ACCESS-S1 allows us to estimate the time-scale over which initial conditions are important. We find

that initial conditions affect Antarctic sea-ice forecasts in the order of a few months, but that effect is seasonally dependent. January to April initial conditions improve forecasts for up to three months. February initial conditions in particular are shown to be crucial for determining sea-ice evolution at least up to May. Arctic sea-ice forecasts
325 also show greater sensitivity to initial conditions in boreal summer, compared with boreal winter (Day et al., 2014; Bunzel et al., 2016), suggesting a similar mechanism might be playing a role.

Forecasts initialised in winter have very little skill and ACCESS-S1 and ACCESS-S2 forecast errors are statistically indistinguishable after just two weeks. This is consistent with Libera et al. (2022)'s finding of a "winter predictability barrier" in the Weddell Sea, although they describe the barrier as a sharp loss of predictability in July, and here we
330 find a gradual reduction in skill compared with climatology around June. This difference might be due to our use of pan-Antarctic RMSE, since our regional analysis indicates that the degraded skill is most dramatic in the King Haakon Sea.

These findings have important implications for both operational forecasting, model development and predictability studies. For operational centers, our results suggest that efforts to improve sea-ice data assimilation should prioritize
335 the summer and autumn months when initial conditions have the greatest impact on forecast skill. Additionally, the substantial bias in ACCESS-S2 highlights the need for improved model physics, particularly in the representation of sea-ice thermodynamics and radiation processes. Crucially, our results suggest dramatic seasonal variations in sea-ice predictability. Future studies should therefore use initial conditions through the whole year rather than focusing on a limited number of initialisation dates.

340 4 References

- Allaire, J., Teague, C., Xie, Y., and Dervieux, C.: Quarto, Zenodo, <https://doi.org/10.5281/ZENODO.5960048>, 2022.
- Best, M. J., Pryor, M., Clark, D. B., Rooney, G. G., Essery, R. L. H., Ménard, C. B., Edwards, J. M., Hendry, M. A., Porson, A., Gedney, N., Mercado, L. M., Sitch, S., Blyth, E., Boucher, O., Cox, P. M., Grimmond, C. S. B., and Harding, R. J.: The Joint UK Land Environment Simulator (JULES), Model Description – Part 1: Energy and Water Fluxes, Geoscientific
345 Model Development, 4, 677–699, <https://doi.org/10.5194/gmd-4-677-2011>, 2011.
- Bunzel, F., Notz, D., Baehr, J., Müller, W. A., and Fröhlich, K.: Seasonal Climate Forecasts Significantly Affected by Observational Uncertainty of Arctic Sea Ice Concentration, Geophysical Research Letters, 43, 852–859,
<https://doi.org/10.1002/2015GL066928>, 2016.
- Campitelli, E.: metR: Tools for Easier Analysis of Meteorological Fields, 2020.
- 350 Campitelli, E.: Data for "Evaluating the Importance of Initial Conditions for Antarctic Sea Ice Seasonal Predictability with a Fully Coupled Forecast Model", <https://doi.org/10.5281/ZENODO.17479537>, 2025.
- Cavalieri, D. J., Gloersen, P., and Campbell, W. J.: Determination of Sea Ice Parameters with the NIMBUS 7 SMMR, Journal of Geophysical Research: Atmospheres, 89, 5355–5369, <https://doi.org/10.1029/JD089iD04p05355>, 1984.

- Cavalieri, D. J., Crawford, J. P., Drinkwater, M. R., Eppler, D. T., Farmer, L. D., Jentz, R. R., and Wackerman, C. C.: Aircraft
355 Active and Passive Microwave Validation of Sea Ice Concentration from the Defense Meteorological Satellite Program Special
Sensor Microwave Imager, *Journal of Geophysical Research: Oceans*, 96, 21 989–22 008, <https://doi.org/10.1029/91JC02335>,
1991.
- Comiso, J.: Bootstrap Sea Ice Concentrations from Nimbus-7 SMMR and DMSP SSM/I-SSMIS. (NSIDC-0079, Version 4).,
<https://doi.org/10.5067/X5LG68MH013O>, 2023.
- 360 Day, J. J., Hawkins, E., and Tietsche, S.: Will Arctic Sea Ice Thickness Initialization Improve Seasonal Forecast Skill?,
Geophysical Research Letters, 41, 7566–7575, <https://doi.org/10.1002/2014GL061694>, 2014.
- De Silva, L. W. A., Inoue, J., Yamaguchi, H., and Terui, T.: Medium Range Sea Ice Prediction in Support of Japanese Research
Vessel MIRAI's Expedition Cruise in 2018, *Polar Geography*, 43, 223–239, <https://doi.org/10.1080/1088937X.2019.1707317>,
2020.
- 365 Dee, D. P., Uppala, S. M., Simmons, A. J., Berrisford, P., Poli, P., Kobayashi, S., Andrae, U., Balmaseda, M. A., Balsamo, G.,
Bauer, P., Bechtold, P., Beljaars, A. C. M., van de Berg, L., Bidlot, J., Bormann, N., Delsol, C., Dragani, R., Fuentes, M.,
Geer, A. J., Haimberger, L., Healy, S. B., Hersbach, H., Hólm, E. V., Isaksen, L., Källberg, P., Köhler, M., Matricardi, M.,
McNally, A. P., Monge-Sanz, B. M., Morcrette, J.-J., Park, B.-K., Peubey, C., de Rosnay, P., Tavolato, C., Thépaut, J.-N.,
and Vitart, F.: The ERA-Interim Reanalysis: Configuration and Performance of the Data Assimilation System, *Quarterly
370 Journal of the Royal Meteorological Society*, 137, 553–597, <https://doi.org/10.1002/qj.828>, 2011.
- Dong, X., Yang, Q., Nie, Y., Zampieri, L., Wang, J., Liu, J., and Chen, D.: Antarctic Sea Ice Prediction with A Convolutional
Long Short-Term Memory Network, *Ocean Modelling*, 190, 102 386, <https://doi.org/10.1016/j.ocemod.2024.102386>, 2024.
- Dowle, M. and Srinivasan, A.: Data.Table: Extension of 'Data.Frame', 2020.
- EUMETSAT Ocean and Sea Ice Satellite Application Facility: Global Sea Ice Concentration Climate Data Record 1978-2020
375 (v3.0, 2022), OSI-450-a.
- Gao, Y., Xiu, Y., Nie, Y., Luo, H., Yang, Q., Zampieri, L., Lv, X., and Uotila, P.: An Assessment of Subseasonal
Prediction Skill of the Antarctic Sea Ice Edge, *Journal of Geophysical Research: Oceans*, 129, e2024JC021499,
<https://doi.org/10.1029/2024JC021499>, 2024.
- Good, S. A., Martin, M. J., and Rayner, N. A.: EN4: Quality Controlled Ocean Temperature and Salinity Profiles and
380 Monthly Objective Analyses with Uncertainty Estimates, *Journal of Geophysical Research: Oceans*, 118, 6704–6716,
<https://doi.org/10.1002/2013JC009067>, 2013.
- Guemas, V., Chevallier, M., Déqué, M., Bellprat, O., and Doblas-Reyes, F.: Impact of Sea Ice Initialization on
Sea Ice and Atmosphere Prediction Skill on Seasonal Timescales, *Geophysical Research Letters*, 43, 3889–3896,
<https://doi.org/10.1002/2015GL066626>, 2016.
- 385 Gurvan, M., Bourdallé-Badie, R., Bouttier, P.-A., Bricaud, C., Bruciaferri, D., Calvert, D., Chanut, J., Clementi, E., Coward,
A., Delrosso, D., Ethé, C., Flavoni, S., Graham, T., Harle, J., Iovino, D., Lea, D., Lévy, C., Lovato, T., Martin, N.,
Masson, S., Mocavero, S., Paul, J., Rousset, C., Storkey, D., Storto, A., and Vancoppenolle, M.: NEMO Ocean Engine,
<https://doi.org/10.5281/zenodo.1475234>, 2013.
- Holland, M. M., Blanchard-Wrigglesworth, E., Kay, J., and Vavrus, S.: Initial-Value Predictability of Antarctic Sea Ice in
390 the Community Climate System Model 3, *Geophysical Research Letters*, 40, 2121–2124, <https://doi.org/10.1002/grl.50410>,
2013.

Hudson, D., Alves, O., Hendon, H. H., Lim, E.-P., Liu, G., Luo, J.-J., MacLachlan, C., Marshall, A. G., Shi, L., Wang, G.,
395 Wedd, R., Young, G., Zhao, M., and Zhou, X.: ACCESS-S1 The New Bureau of Meteorology Multi-Week to Seasonal
Prediction System, *Journal of Southern Hemisphere Earth Systems Science*, 67, 132–159, <https://doi.org/10.1071/es17009>,
2017.

Libera, S., Hobbs, W., Klocker, A., Meyer, A., and Matear, R.: Ocean-Sea Ice Processes and Their
Role in Multi-Month Predictability of Antarctic Sea Ice, *Geophysical Research Letters*, 49, e2021GL097047,
<https://doi.org/10.1029/2021GL097047>, 2022.

Lin, Y., Yang, Q., Li, X., Dong, X., Luo, H., Nie, Y., Wang, J., Wang, Y., and Min, C.: Ice-kNN-South: A Lightweight Machine
400 Learning Model for Antarctic Sea Ice Prediction, *Journal of Geophysical Research: Machine Learning and Computation*, 2,
e2024JH000433, <https://doi.org/10.1029/2024JH000433>, 2025.

Marchi, S., Fichefet, T., and Goosse, H.: Respective Influences of Perturbed Atmospheric and Ocean–Sea Ice Initial Conditions
on the Skill of Seasonal Antarctic Sea Ice Predictions: A Study with NEMO3.6–LIM3, *Ocean Modelling*, 148, 101591,
<https://doi.org/10.1016/j.ocemod.2020.101591>, 2020.

405 Massonnet, F., Barreira, S., Barthélémy, A., Bilbao, R., Blanchard-Wrigglesworth, E., Blockley, E., Bromwich, D. H., Bushuk,
M., Dong, X., Goessling, H. F., Hobbs, W., Iovino, D., Lee, W.-S., Li, C., Meier, W. N., Merryfield, W. J., Moreno-Chamarro,
E., Morioka, Y., Li, X., Niraula, B., Petty, A., Sanna, A., Scilingo, M., Shu, Q., Sigmond, M., Sun, N., Tietsche, S., Wu, X.,
Yang, Q., and Yuan, X.: SIPN South: Six Years of Coordinated Seasonal Antarctic Sea Ice Predictions, *Frontiers in Marine
Science*, 10, <https://doi.org/10.3389/fmars.2023.1148899>, 2023.

410 Megann, A., Storkey, D., Aksenov, Y., Alderson, S., Calvert, D., Graham, T., Hyder, P., Siddorn, J., and Sinha, B.: GO5.0:
The Joint NERC–Met Office NEMO Global Ocean Model for Use in Coupled and Forced Applications, *Geoscientific Model
Development*, 7, 1069–1092, <https://doi.org/10.5194/gmd-7-1069-2014>, 2014.

Meier, W. N. and Stewart, J. S.: Assessing Uncertainties in Sea Ice Extent Climate Indicators, *Environmental Research Letters*,
14, 035005, <https://doi.org/10.1088/1748-9326/aaf52c>, 2019.

415 Meier, W. N., Peng, G., Scott, D. J., and Savoie, M. H.: Verification of a New NOAA/NSIDC Passive Microwave Sea-Ice
Concentration Climate Record, *Polar Research*, <https://doi.org/10.3402/polar.v33.21004>, 2014.

Meier, W. N., Fetterer, F., Windnagel, A. K., and Stewart, J. S.: NOAA/NSIDC Climate Data Record of Passive Microwave
Sea Ice Concentration, <https://doi.org/10.7265/efmz-2t65>, 2021.

Morioka, Y., Iovino, D., Cipollone, A., Masina, S., and Behera, S. K.: Decadal Sea Ice Prediction in the West Antarctic Seas
420 with Ocean and Sea Ice Initializations, *Communications Earth & Environment*, 3, 189, [https://doi.org/10.1038/s43247-022-00529-z](https://doi.org/10.1038/s43247-022-
00529-z), 2022.

Murphy, A. H. and Daan, H.: Forecast Evaluation, in: *Probability, Statistics, And Decision Making In The Atmospheric
Sciences*, CRC Press, 1985.

R Core Team: R: A Language and Environment for Statistical Computing, R Foundation for Statistical Computing, Vienna,
425 Austria, 2020.

Rae, J. G. L., Hewitt, H. T., Keen, A. B., Ridley, J. K., West, A. E., Harris, C. M., Hunke, E. C., and Walters, D. N.:
Development of the Global Sea Ice 6.0 CICE Configuration for the Met Office Global Coupled Model, *Geoscientific Model
Development*, 8, 2221–2230, <https://doi.org/10.5194/gmd-8-2221-2015>, 2015.

- Reynolds, R. W., Smith, T. M., Liu, C., Chelton, D. B., Casey, K. S., and Schlax, M. G.: Daily High-Resolution-Blended Analyses for Sea Surface Temperature, *Journal of Climate*, 20, 5473–5496, <https://doi.org/10.1175/2007JCLI1824.1>, 2007.
- Rinke, A., Maslowski, W., Dethloff, K., and Clement, J.: Influence of Sea Ice on the Atmosphere: A Study with an Arctic Atmospheric Regional Climate Model, *Journal of Geophysical Research: Atmospheres*, 111, <https://doi.org/10.1029/2005JD006957>, 2006.
- Roach, L. A., Dörr, J., Holmes, C. R., Massonnet, F., Blockley, E. W., Notz, D., Rackow, T., Raphael, M. N., O'Farrell, S. P., Bailey, D. A., and Bitz, C. M.: Antarctic Sea Ice Area in CMIP6, *Geophysical Research Letters*, 47, e2019GL086729, <https://doi.org/10.1029/2019GL086729>, 2020.
- Schulzweida, U.: CDO User Guide, <https://doi.org/10.5281/ZENODO.10020800>, 2023.
- Semmler, T., Kasper, M. A., Jung, T., and Serrar, S.: Remote Impact of the Antarctic Atmosphere on the Southern Mid?Latitudes, *Meteorologische Zeitschrift*, 25, 71–77, <https://doi.org/10.1127/metz/2015/0685>, 2016.
- Wagner, P. M., Hughes, N., Bourbonnais, P., Stroeve, J., Rabenstein, L., Bhatt, U., Little, J., Wiggins, H., and Fleming, A.: Sea-Ice Information and Forecast Needs for Industry Maritime Stakeholders, *Polar Geography*, 43, 160–187, <https://doi.org/10.1080/1088937X.2020.1766592>, 2020.
- Wang, Z., Fraser, A. D., Reid, P., Coleman, R., and O'Farrell, S.: The Influence of Time-Varying Sea Ice Concentration on Antarctic and Southern Ocean Numerical Weather Prediction, *Weather and Forecasting*, 39, 293–310, <https://doi.org/10.1175/WAF-D-22-0220.1>, 2024.
- Waters, J., Lea, D. J., Martin, M. J., Mirouze, I., Weaver, A., and While, J.: Implementing a Variational Data Assimilation System in an Operational 1/4 Degree Global Ocean Model, *Quarterly Journal of the Royal Meteorological Society*, 141, 333–349, <https://doi.org/10.1002/qj.2388>, 2015.
- Waters, J., Bell, M. J., Martin, M. J., and Lea, D. J.: Reducing Ocean Model Imbalances in the Equatorial Region Caused by Data Assimilation, *Quarterly Journal of the Royal Meteorological Society*, 143, 195–208, <https://doi.org/10.1002/qj.2912>, 2017.
- Wedd, R., Alves, O., de Burgh-Day, C., Down, C., Griffiths, M., Hendon, H. H., Hudson, D., Li, S., Lim, E.-P., Marshall, A. G., Shi, L., Smith, P., Smith, G., Spillman, C. M., Wang, G., Wheeler, M. C., Yan, H., Yin, Y., Young, G., Zhao, M., Xiao, Y., and Zhou, X.: ACCESS-S2: The Upgraded Bureau of Meteorology Multi-Week to Seasonal Prediction System, *Journal of Southern Hemisphere Earth Systems Science*, 72, 218–242, <https://doi.org/10.1071/ES22026>, 2022.
- Wickham, H.: Ggplot2: Elegant Graphics for Data Analysis, Use R!, Springer-Verlag, New York, <https://doi.org/10.1007/978-0-387-98141-3>, 2009.
- Williams, K. D., Harris, C. M., Bodas-Salcedo, A., Camp, J., Comer, R. E., Copsey, D., Fereday, D., Graham, T., Hill, R., Hinton, T., Hyder, P., Ineson, S., Masato, G., Milton, S. F., Roberts, M. J., Rowell, D. P., Sanchez, C., Shelly, A., Sinha, B., Walters, D. N., West, A., Woollings, T., and Xavier, P. K.: The Met Office Global Coupled Model 2.0 (GC2) Configuration, *Geoscientific Model Development*, 8, 1509–1524, <https://doi.org/10.5194/gmd-8-1509-2015>, 2015.
- Xie, Y.: Dynamic Documents with R and Knitr, Chapman and Hall/CRC, Boca Raton, Florida, 2 edn., 2015.
- Zampieri, L., Goessling, H. F., and Jung, T.: Predictability of Antarctic Sea Ice Edge on Subseasonal Time Scales, *Geophysical Research Letters*, 46, 9719–9727, <https://doi.org/10.1029/2019GL084096>, 2019.
- Zhou, X. and Alves, O.: Evaluating Sea Ice in ACCESS-S2, Tech. rep., Bureau of Meteorology, 2022.

Zweng, M. M., Reagan, J. R., Antonov, J. I., Locarnini, R. A., Mishonov, A. V., Boyer, T. P., Garcia, H. E., Baranova, O. K., Johnson, D. R., Seidov, D., and Biddle, M. M.: World Ocean Atlas 2013. Volume 2, Salinity, <https://doi.org/10.7289/V5251G4D>, 2013.

5 Appendix

470 The following are the same figures from the main paper but using the OSI dataset instead of CDR.

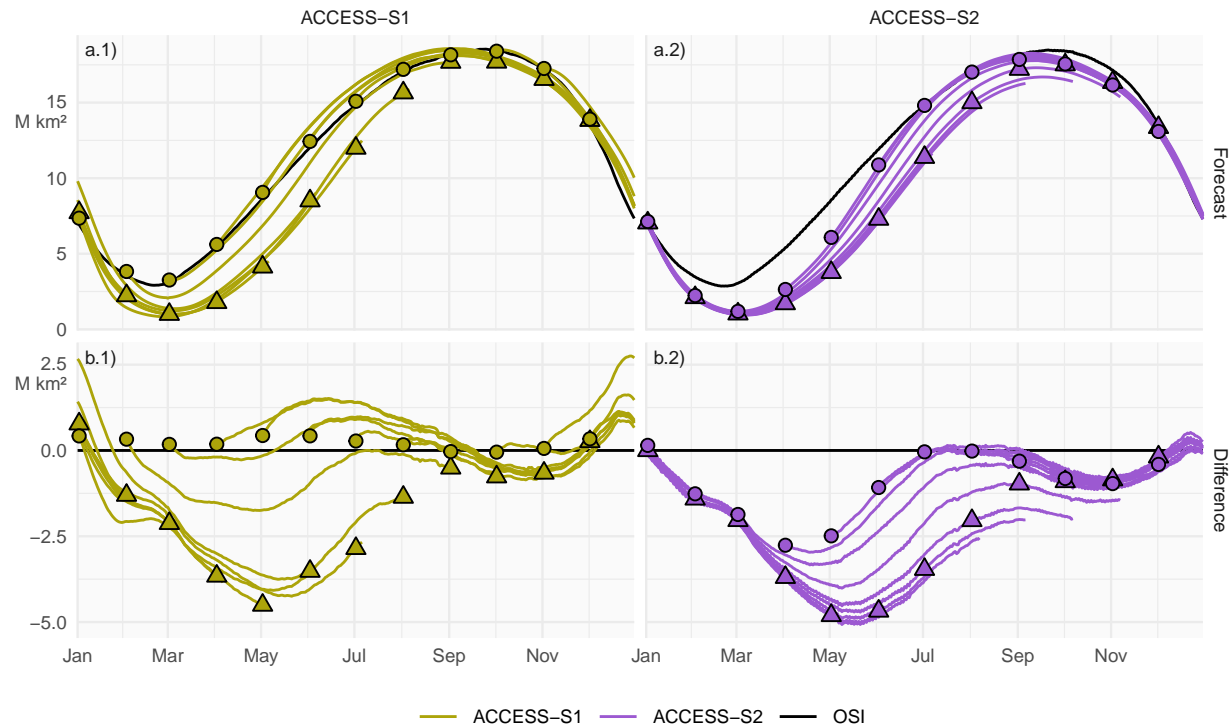


Figure A1. Row a: Pan-Antarctic daily mean sea-ice extent for all hindcasts initialised on the first of each calendar month for ACCESS-S1 (column 1; green) and ACCESS-S2 (column 2; purple). Observed mean sea-ice extent in each corresponding hindcast period is shown in black. Row b: Mean differences between the forecast and the observed values. Circles represent the initial conditions at the start of forecasts (i.e., the first of every month), and triangles represent the mean values at the lead time corresponding to the maximum lead time in S1 (between 213 and 216 days, depending on the month)

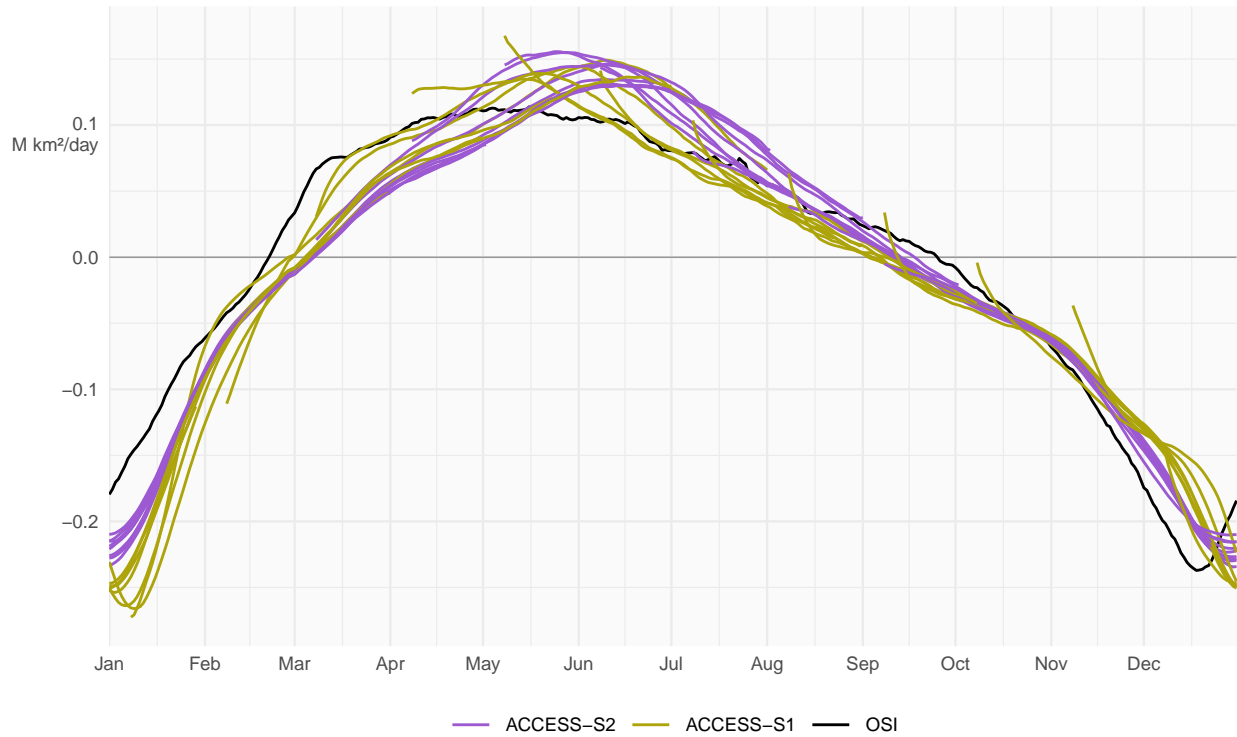


Figure A2. Mean daily sea-ice extent growth ($10^6 \text{ km}^2/\text{day}$) in ACCESS-S1 (green) and ACCESS-S2 (purple) hindcasts and observations (black), computed as the mean daily differences in sea-ice extent between each date and the next for each forecast month. Values are smoothed with a 11-day running mean.

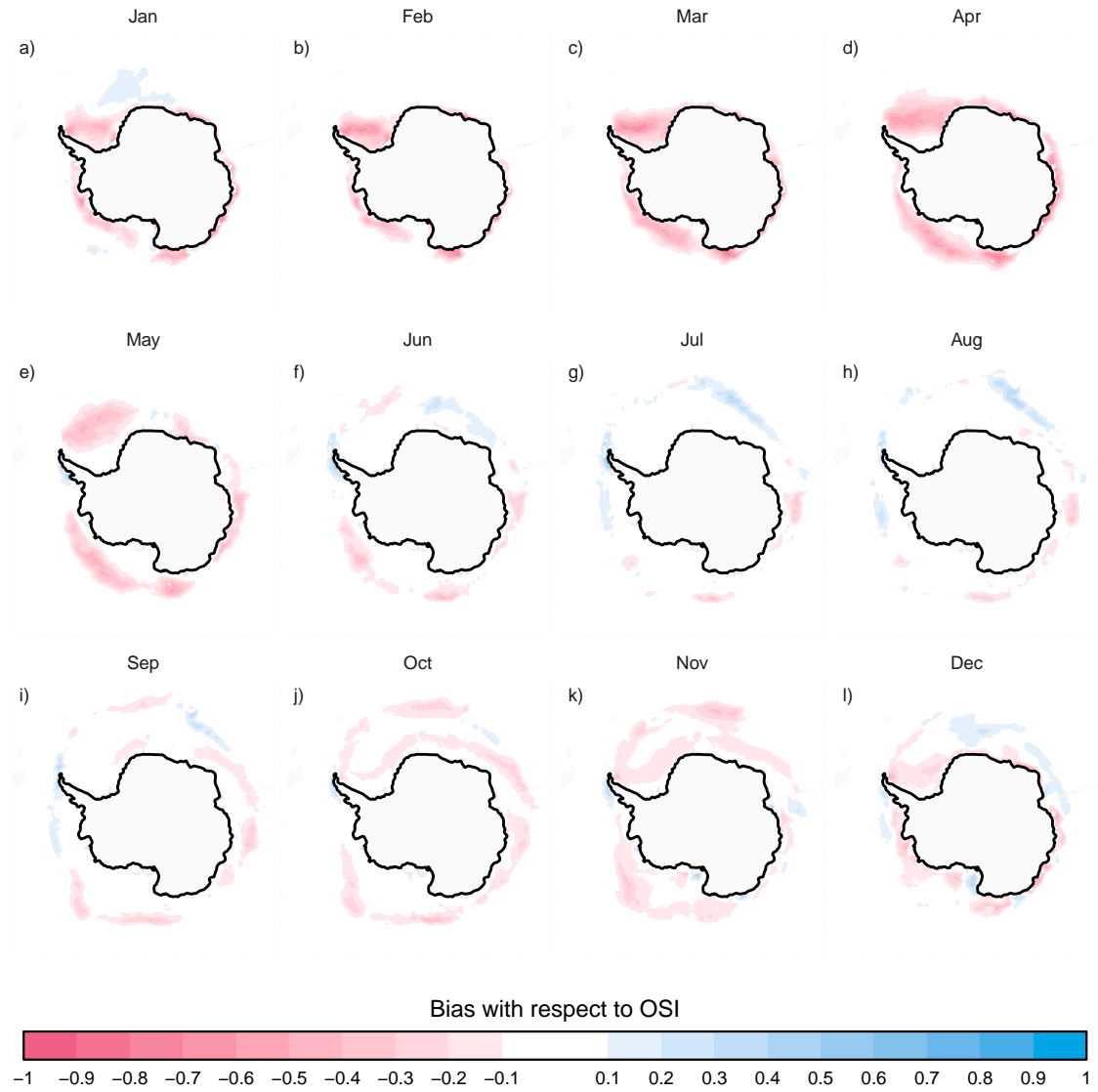


Figure A3. Ensemble mean difference between monthly sea-ice concentration of ACCESS-S2 ensemble mean forecast at 0-month lead time (monthly mean values forecasted from the forecast initialised at the first of the month) and observations (OSI).

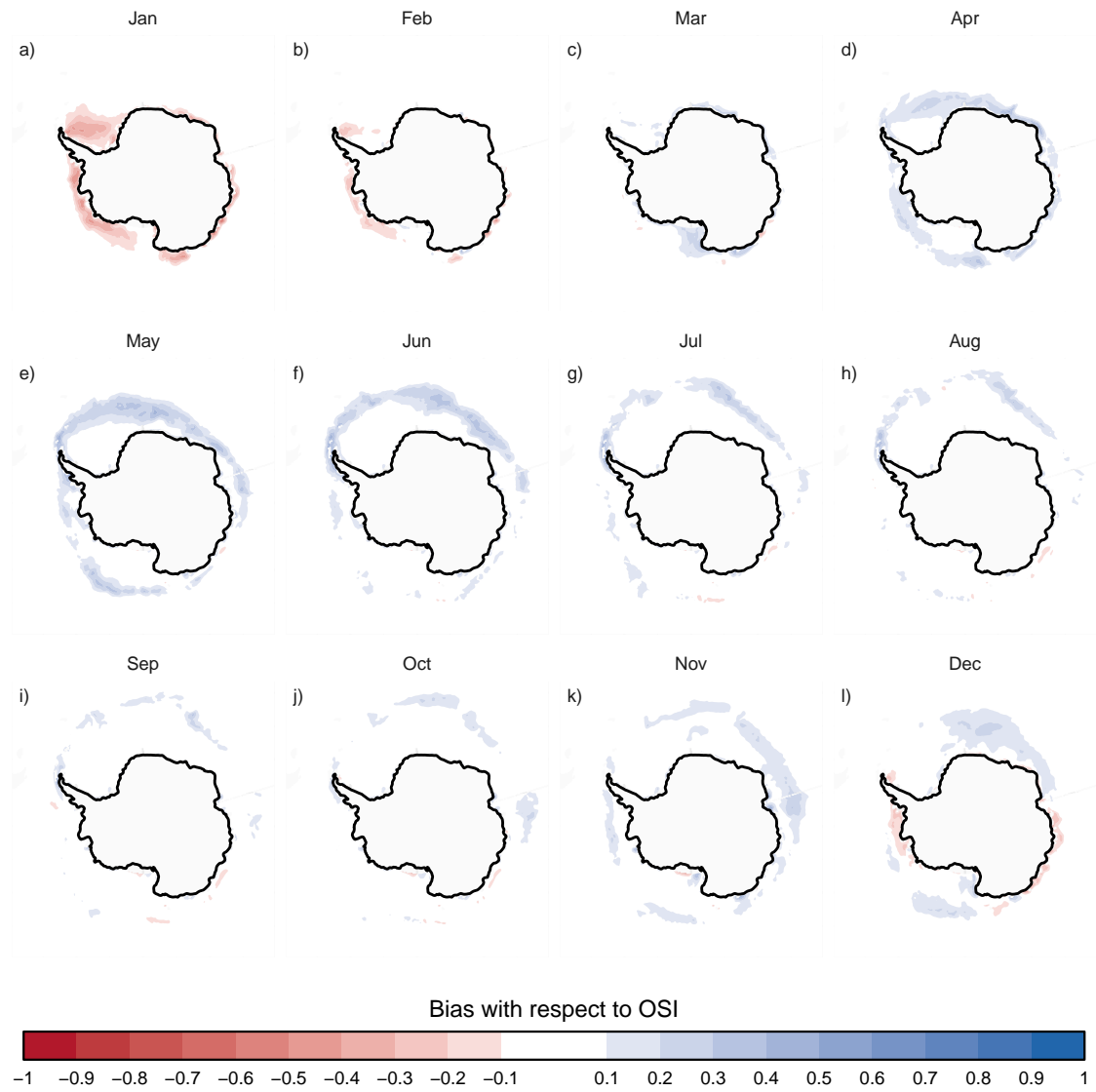


Figure A4. Same as Figure 3 but for ACCESS-S1.

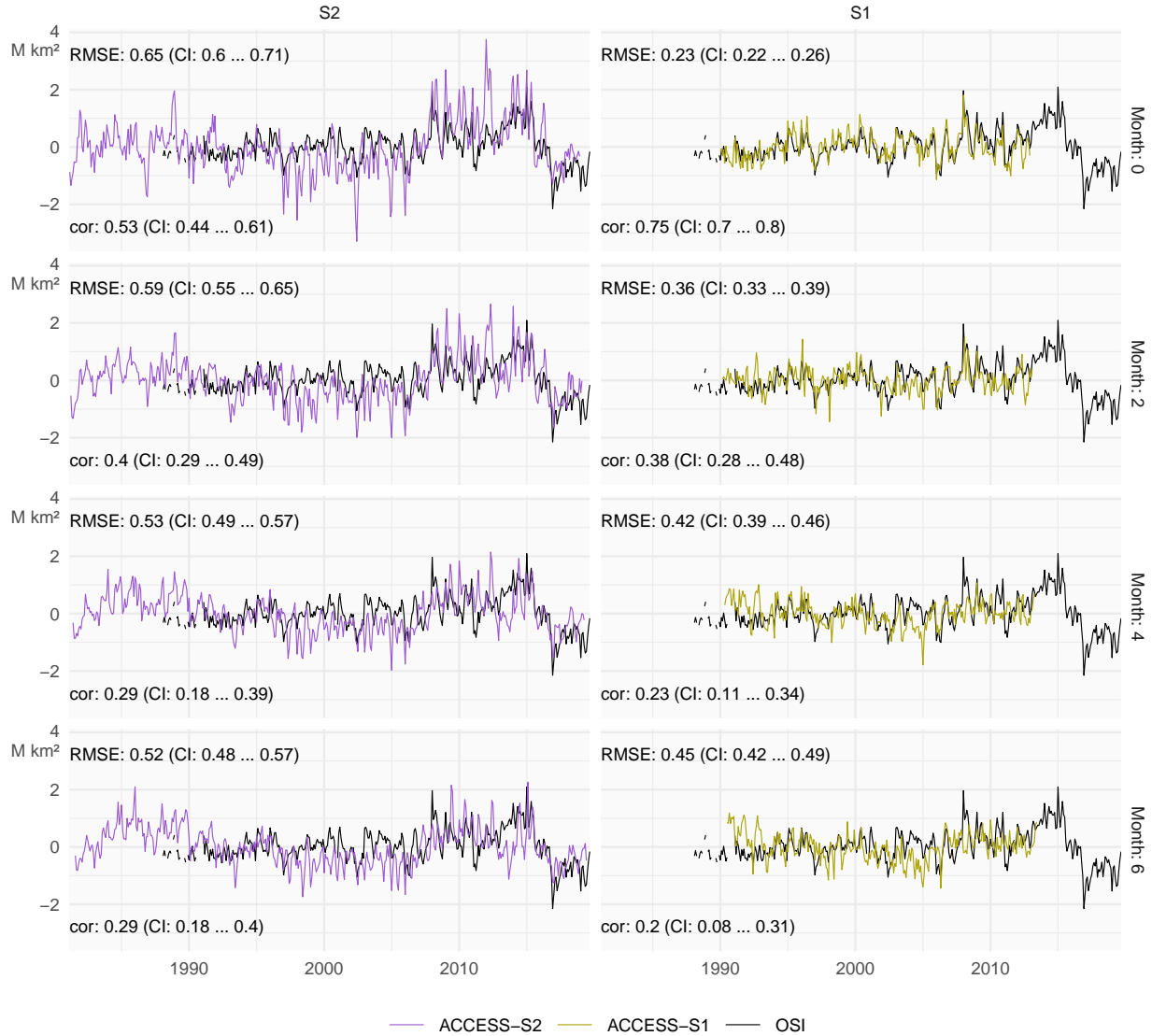


Figure A5. Monthly mean sea-ice extent anomalies of the observations (black) and forecasts from ACCESS-S1 (right column; purple) and ACCESS-S2 (left column; green) at lead times of 0, 2, 4, and 6 months. The RMSE and correlation with their respective 95% confidence interval during the overlapping period of ACCESS-S1 and ACCESS-S2 hindcasts (1990–2013) are shown on the top left and bottom left of each panel respectively

```

$data
$data[[1]]

  colour x      y PANEL group flipped_aes linewidth linetype alpha
1 #9C59D1 -9 0.5984605 1     1 FALSE    0.5       1 NA
475 2 #9C59D1 -8 0.4772937 1     1 FALSE    0.5       1 NA
3 #9C59D1 -7 0.6183552 1     1 FALSE    0.5       1 NA
4 #9C59D1 -6 0.6039833 1     1 FALSE    0.5       1 NA
5 #9C59D1 -5 0.6250643 1     1 FALSE    0.5       1 NA
6 #9C59D1 -4 0.7092255 1     1 FALSE    0.5       1 NA
480 7 #9C59D1 -3 0.7552064 1     1 FALSE    0.5       1 NA
8 #9C59D1 -2 0.9081425 1     1 FALSE    0.5       1 NA
9 #9C59D1 -1 1.0889439 1     1 FALSE    0.5       1 NA
10 #9C59D1 0 1.1941767 1     1 FALSE    0.5       1 NA
11 #ACA40A -7 0.7565361 1     2 FALSE    0.5       1 NA
485 12 #ACA40A -6 0.5959845 1     2 FALSE    0.5       1 NA
13 #ACA40A -5 0.5955162 1     2 FALSE    0.5       1 NA
14 #ACA40A -4 0.4812004 1     2 FALSE    0.5       1 NA
15 #ACA40A -3 0.6866438 1     2 FALSE    0.5       1 NA
16 #ACA40A -2 0.4878597 1     2 FALSE    0.5       1 NA
490 17 #ACA40A -1 0.3958258 1     2 FALSE    0.5       1 NA
18 #ACA40A 0 0.2482179 1     2 FALSE    0.5       1 NA
19 #9C59D1 -9 0.4784391 2     1 FALSE    0.5       1 NA
20 #9C59D1 -8 0.4578146 2     1 FALSE    0.5       1 NA
21 #9C59D1 -7 0.4339634 2     1 FALSE    0.5       1 NA
495 22 #9C59D1 -6 0.4779146 2     1 FALSE    0.5       1 NA
23 #9C59D1 -5 0.5586558 2     1 FALSE    0.5       1 NA
24 #9C59D1 -4 0.5645042 2     1 FALSE    0.5       1 NA
25 #9C59D1 -3 0.5796230 2     1 FALSE    0.5       1 NA
26 #9C59D1 -2 0.8235551 2     1 FALSE    0.5       1 NA
500 27 #9C59D1 -1 0.8542623 2     1 FALSE    0.5       1 NA
28 #9C59D1 0 0.6718616 2     1 FALSE    0.5       1 NA
29 #ACA40A -7 0.5247870 2     2 FALSE    0.5       1 NA
30 #ACA40A -6 0.5405390 2     2 FALSE    0.5       1 NA
31 #ACA40A -5 0.4929244 2     2 FALSE    0.5       1 NA
505 32 #ACA40A -4 0.4194970 2     2 FALSE    0.5       1 NA

```

33	#ACA40A	-3	0.4611708	2	2	FALSE	0.5	1	NA	
34	#ACA40A	-2	0.5108275	2	2	FALSE	0.5	1	NA	
35	#ACA40A	-1	0.2220359	2	2	FALSE	0.5	1	NA	
36	#ACA40A	0	0.1245617	2	2	FALSE	0.5	1	NA	
510	37	#9C59D1	-9	0.4207578	3	1	FALSE	0.5	1	NA
	38	#9C59D1	-8	0.4177998	3	1	FALSE	0.5	1	NA
	39	#9C59D1	-7	0.4165393	3	1	FALSE	0.5	1	NA
	40	#9C59D1	-6	0.4958292	3	1	FALSE	0.5	1	NA
	41	#9C59D1	-5	0.4837393	3	1	FALSE	0.5	1	NA
515	42	#9C59D1	-4	0.4255676	3	1	FALSE	0.5	1	NA
	43	#9C59D1	-3	0.4514970	3	1	FALSE	0.5	1	NA
	44	#9C59D1	-2	0.4883231	3	1	FALSE	0.5	1	NA
	45	#9C59D1	-1	0.4978986	3	1	FALSE	0.5	1	NA
	46	#9C59D1	0	0.4856632	3	1	FALSE	0.5	1	NA
520	47	#ACA40A	-7	0.4558333	3	2	FALSE	0.5	1	NA
	48	#ACA40A	-6	0.4103865	3	2	FALSE	0.5	1	NA
	49	#ACA40A	-5	0.3550077	3	2	FALSE	0.5	1	NA
	50	#ACA40A	-4	0.3637343	3	2	FALSE	0.5	1	NA
	51	#ACA40A	-3	0.3655096	3	2	FALSE	0.5	1	NA
525	52	#ACA40A	-2	0.2600277	3	2	FALSE	0.5	1	NA
	53	#ACA40A	-1	0.1856420	3	2	FALSE	0.5	1	NA
	54	#ACA40A	0	0.1034259	3	2	FALSE	0.5	1	NA
	55	#9C59D1	-9	0.4748831	4	1	FALSE	0.5	1	NA
	56	#9C59D1	-8	0.5165270	4	1	FALSE	0.5	1	NA
530	57	#9C59D1	-7	0.5554201	4	1	FALSE	0.5	1	NA
	58	#9C59D1	-6	0.5624090	4	1	FALSE	0.5	1	NA
	59	#9C59D1	-5	0.4981750	4	1	FALSE	0.5	1	NA
	60	#9C59D1	-4	0.5348628	4	1	FALSE	0.5	1	NA
	61	#9C59D1	-3	0.6254053	4	1	FALSE	0.5	1	NA
535	62	#9C59D1	-2	0.6286052	4	1	FALSE	0.5	1	NA
	63	#9C59D1	-1	0.6668942	4	1	FALSE	0.5	1	NA
	64	#9C59D1	0	0.8824187	4	1	FALSE	0.5	1	NA
	65	#ACA40A	-7	0.4521898	4	2	FALSE	0.5	1	NA
	66	#ACA40A	-6	0.3974993	4	2	FALSE	0.5	1	NA
540	67	#ACA40A	-5	0.4270625	4	2	FALSE	0.5	1	NA

68	#ACA40A	-4	0.4026673	4	2	FALSE	0.5	1	NA	
69	#ACA40A	-3	0.3582458	4	2	FALSE	0.5	1	NA	
70	#ACA40A	-2	0.2900451	4	2	FALSE	0.5	1	NA	
71	#ACA40A	-1	0.2854501	4	2	FALSE	0.5	1	NA	
545	72	#ACA40A	0	0.1821203	4	2	FALSE	0.5	1	NA
	73	#9C59D1	-9	0.5579666	5	1	FALSE	0.5	1	NA
	74	#9C59D1	-8	0.6127165	5	1	FALSE	0.5	1	NA
	75	#9C59D1	-7	0.6029918	5	1	FALSE	0.5	1	NA
	76	#9C59D1	-6	0.5841198	5	1	FALSE	0.5	1	NA
550	77	#9C59D1	-5	0.7928835	5	1	FALSE	0.5	1	NA
	78	#9C59D1	-4	0.8556750	5	1	FALSE	0.5	1	NA
	79	#9C59D1	-3	0.8069800	5	1	FALSE	0.5	1	NA
	80	#9C59D1	-2	0.8437517	5	1	FALSE	0.5	1	NA
	81	#9C59D1	-1	1.0196410	5	1	FALSE	0.5	1	NA
555	82	#9C59D1	0	1.1065527	5	1	FALSE	0.5	1	NA
	83	#ACA40A	-7	0.4807941	5	2	FALSE	0.5	1	NA
	84	#ACA40A	-6	0.5067542	5	2	FALSE	0.5	1	NA
	85	#ACA40A	-5	0.5393445	5	2	FALSE	0.5	1	NA
	86	#ACA40A	-4	0.4045959	5	2	FALSE	0.5	1	NA
560	87	#ACA40A	-3	0.3845793	5	2	FALSE	0.5	1	NA
	88	#ACA40A	-2	0.3869069	5	2	FALSE	0.5	1	NA
	89	#ACA40A	-1	0.2904025	5	2	FALSE	0.5	1	NA
	90	#ACA40A	0	0.3350960	5	2	FALSE	0.5	1	NA
	91	#9C59D1	-9	0.6660617	6	1	FALSE	0.5	1	NA
565	92	#9C59D1	-8	0.6701446	6	1	FALSE	0.5	1	NA
	93	#9C59D1	-7	0.7190907	6	1	FALSE	0.5	1	NA
	94	#9C59D1	-6	0.9407559	6	1	FALSE	0.5	1	NA
	95	#9C59D1	-5	1.0161669	6	1	FALSE	0.5	1	NA
	96	#9C59D1	-4	0.8244582	6	1	FALSE	0.5	1	NA
570	97	#9C59D1	-3	0.8373873	6	1	FALSE	0.5	1	NA
	98	#9C59D1	-2	0.9105125	6	1	FALSE	0.5	1	NA
	99	#9C59D1	-1	0.8492269	6	1	FALSE	0.5	1	NA
	100	#9C59D1	0	0.7665951	6	1	FALSE	0.5	1	NA
	101	#ACA40A	-7	0.5531898	6	2	FALSE	0.5	1	NA
575	102	#ACA40A	-6	0.5026169	6	2	FALSE	0.5	1	NA

	103	#ACA40A	-5	0.4387233	6	2	FALSE	0.5	1	NA
	104	#ACA40A	-4	0.5029235	6	2	FALSE	0.5	1	NA
	105	#ACA40A	-3	0.4217662	6	2	FALSE	0.5	1	NA
	106	#ACA40A	-2	0.3496994	6	2	FALSE	0.5	1	NA
580	107	#ACA40A	-1	0.3387964	6	2	FALSE	0.5	1	NA
	108	#ACA40A	0	0.4231441	6	2	FALSE	0.5	1	NA
	109	#9C59D1	-9	0.6450049	7	1	FALSE	0.5	1	NA
	110	#9C59D1	-8	0.7003431	7	1	FALSE	0.5	1	NA
	111	#9C59D1	-7	0.8720344	7	1	FALSE	0.5	1	NA
585	112	#9C59D1	-6	0.9102250	7	1	FALSE	0.5	1	NA
	113	#9C59D1	-5	0.6764296	7	1	FALSE	0.5	1	NA
	114	#9C59D1	-4	0.6273290	7	1	FALSE	0.5	1	NA
	115	#9C59D1	-3	0.5766315	7	1	FALSE	0.5	1	NA
	116	#9C59D1	-2	0.4778696	7	1	FALSE	0.5	1	NA
590	117	#9C59D1	-1	0.4421313	7	1	FALSE	0.5	1	NA
	118	#9C59D1	0	0.3340629	7	1	FALSE	0.5	1	NA
	119	#ACA40A	-7	0.3926180	7	2	FALSE	0.5	1	NA
	120	#ACA40A	-6	0.4055218	7	2	FALSE	0.5	1	NA
	121	#ACA40A	-5	0.4615250	7	2	FALSE	0.5	1	NA
595	122	#ACA40A	-4	0.4564888	7	2	FALSE	0.5	1	NA
	123	#ACA40A	-3	0.3854216	7	2	FALSE	0.5	1	NA
	124	#ACA40A	-2	0.3252267	7	2	FALSE	0.5	1	NA
	125	#ACA40A	-1	0.4481883	7	2	FALSE	0.5	1	NA
	126	#ACA40A	0	0.3257066	7	2	FALSE	0.5	1	NA
600	127	#9C59D1	-9	0.5283287	8	1	FALSE	0.5	1	NA
	128	#9C59D1	-8	0.6052768	8	1	FALSE	0.5	1	NA
	129	#9C59D1	-7	0.6068318	8	1	FALSE	0.5	1	NA
	130	#9C59D1	-6	0.4303770	8	1	FALSE	0.5	1	NA
	131	#9C59D1	-5	0.4173341	8	1	FALSE	0.5	1	NA
605	132	#9C59D1	-4	0.3923987	8	1	FALSE	0.5	1	NA
	133	#9C59D1	-3	0.3123127	8	1	FALSE	0.5	1	NA
	134	#9C59D1	-2	0.3363830	8	1	FALSE	0.5	1	NA
	135	#9C59D1	-1	0.2675447	8	1	FALSE	0.5	1	NA
	136	#9C59D1	0	0.3365351	8	1	FALSE	0.5	1	NA
610	137	#ACA40A	-7	0.3268014	8	2	FALSE	0.5	1	NA

	138	#ACA40A	-6	0.3875728	8	2	FALSE	0.5	1	NA
	139	#ACA40A	-5	0.4307579	8	2	FALSE	0.5	1	NA
	140	#ACA40A	-4	0.3423391	8	2	FALSE	0.5	1	NA
	141	#ACA40A	-3	0.3293139	8	2	FALSE	0.5	1	NA
615	142	#ACA40A	-2	0.3821151	8	2	FALSE	0.5	1	NA
	143	#ACA40A	-1	0.3452069	8	2	FALSE	0.5	1	NA
	144	#ACA40A	0	0.2554071	8	2	FALSE	0.5	1	NA
	145	#9C59D1	-9	0.4812590	9	1	FALSE	0.5	1	NA
	146	#9C59D1	-8	0.4743413	9	1	FALSE	0.5	1	NA
620	147	#9C59D1	-7	0.4297590	9	1	FALSE	0.5	1	NA
	148	#9C59D1	-6	0.3962710	9	1	FALSE	0.5	1	NA
	149	#9C59D1	-5	0.3600449	9	1	FALSE	0.5	1	NA
	150	#9C59D1	-4	0.3618450	9	1	FALSE	0.5	1	NA
	151	#9C59D1	-3	0.3679888	9	1	FALSE	0.5	1	NA
625	152	#9C59D1	-2	0.3721232	9	1	FALSE	0.5	1	NA
	153	#9C59D1	-1	0.3502792	9	1	FALSE	0.5	1	NA
	154	#9C59D1	0	0.3480131	9	1	FALSE	0.5	1	NA
	155	#ACA40A	-7	0.4420522	9	2	FALSE	0.5	1	NA
	156	#ACA40A	-6	0.4766696	9	2	FALSE	0.5	1	NA
630	157	#ACA40A	-5	0.4193247	9	2	FALSE	0.5	1	NA
	158	#ACA40A	-4	0.4452902	9	2	FALSE	0.5	1	NA
	159	#ACA40A	-3	0.4194858	9	2	FALSE	0.5	1	NA
	160	#ACA40A	-2	0.3148970	9	2	FALSE	0.5	1	NA
	161	#ACA40A	-1	0.2736958	9	2	FALSE	0.5	1	NA
635	162	#ACA40A	0	0.1977477	9	2	FALSE	0.5	1	NA
	163	#9C59D1	-9	0.4864481	10	1	FALSE	0.5	1	NA
	164	#9C59D1	-8	0.4592050	10	1	FALSE	0.5	1	NA
	165	#9C59D1	-7	0.4305820	10	1	FALSE	0.5	1	NA
	166	#9C59D1	-6	0.3583702	10	1	FALSE	0.5	1	NA
640	167	#9C59D1	-5	0.3875961	10	1	FALSE	0.5	1	NA
	168	#9C59D1	-4	0.3831390	10	1	FALSE	0.5	1	NA
	169	#9C59D1	-3	0.4452131	10	1	FALSE	0.5	1	NA
	170	#9C59D1	-2	0.3898225	10	1	FALSE	0.5	1	NA
	171	#9C59D1	-1	0.4459450	10	1	FALSE	0.5	1	NA
645	172	#9C59D1	0	0.4557616	10	1	FALSE	0.5	1	NA

	173	#ACA40A	-7	0.5307289	10	2	FALSE	0.5	1	NA
	174	#ACA40A	-6	0.4979372	10	2	FALSE	0.5	1	NA
	175	#ACA40A	-5	0.5037229	10	2	FALSE	0.5	1	NA
	176	#ACA40A	-4	0.5176257	10	2	FALSE	0.5	1	NA
650	177	#ACA40A	-3	0.3819866	10	2	FALSE	0.5	1	NA
	178	#ACA40A	-2	0.3222078	10	2	FALSE	0.5	1	NA
	179	#ACA40A	-1	0.2436012	10	2	FALSE	0.5	1	NA
	180	#ACA40A	0	0.2279954	10	2	FALSE	0.5	1	NA
	181	#9C59D1	-9	0.3978157	11	1	FALSE	0.5	1	NA
655	182	#9C59D1	-8	0.3974092	11	1	FALSE	0.5	1	NA
	183	#9C59D1	-7	0.3097370	11	1	FALSE	0.5	1	NA
	184	#9C59D1	-6	0.3419708	11	1	FALSE	0.5	1	NA
	185	#9C59D1	-5	0.3765437	11	1	FALSE	0.5	1	NA
	186	#9C59D1	-4	0.3672185	11	1	FALSE	0.5	1	NA
660	187	#9C59D1	-3	0.3915742	11	1	FALSE	0.5	1	NA
	188	#9C59D1	-2	0.5181415	11	1	FALSE	0.5	1	NA
	189	#9C59D1	-1	0.4613723	11	1	FALSE	0.5	1	NA
	190	#9C59D1	0	0.6167969	11	1	FALSE	0.5	1	NA
	191	#ACA40A	-7	0.4989726	11	2	FALSE	0.5	1	NA
665	192	#ACA40A	-6	0.4803765	11	2	FALSE	0.5	1	NA
	193	#ACA40A	-5	0.4394459	11	2	FALSE	0.5	1	NA
	194	#ACA40A	-4	0.3776623	11	2	FALSE	0.5	1	NA
	195	#ACA40A	-3	0.3166791	11	2	FALSE	0.5	1	NA
	196	#ACA40A	-2	0.2624609	11	2	FALSE	0.5	1	NA
670	197	#ACA40A	-1	0.2813278	11	2	FALSE	0.5	1	NA
	198	#ACA40A	0	0.1675816	11	2	FALSE	0.5	1	NA
	199	#9C59D1	-9	0.3440246	12	1	FALSE	0.5	1	NA
	200	#9C59D1	-8	0.3907403	12	1	FALSE	0.5	1	NA
	201	#9C59D1	-7	0.3898249	12	1	FALSE	0.5	1	NA
675	202	#9C59D1	-6	0.3972901	12	1	FALSE	0.5	1	NA
	203	#9C59D1	-5	0.4323504	12	1	FALSE	0.5	1	NA
	204	#9C59D1	-4	0.4684049	12	1	FALSE	0.5	1	NA
	205	#9C59D1	-3	0.6148242	12	1	FALSE	0.5	1	NA
	206	#9C59D1	-2	0.5959746	12	1	FALSE	0.5	1	NA
680	207	#9C59D1	-1	0.6667716	12	1	FALSE	0.5	1	NA

208	#9C59D1	0	0.8636783	12	1	FALSE	0.5	1	NA	
209	#ACA40A	-7	0.4544102	12	2	FALSE	0.5	1	NA	
210	#ACA40A	-6	0.4791325	12	2	FALSE	0.5	1	NA	
211	#ACA40A	-5	0.4166218	12	2	FALSE	0.5	1	NA	
685	212	#ACA40A	-4	0.3897752	12	2	FALSE	0.5	1	NA
	213	#ACA40A	-3	0.4265074	12	2	FALSE	0.5	1	NA
	214	#ACA40A	-2	0.3779267	12	2	FALSE	0.5	1	NA
	215	#ACA40A	-1	0.3372106	12	2	FALSE	0.5	1	NA
	216	#ACA40A	0	0.1711289	12	2	FALSE	0.5	1	NA

690

```
$layout
<ggproto object: Class Layout, gg>
  coord: <ggproto object: Class CoordCartesian, Coord, gg>
695    aspect: function
    backtransform_range: function
    clip: on
    default: TRUE
    distance: function
700    expand: TRUE
    is_free: function
    is_linear: function
    labels: function
    limits: list
705    modify_scales: function
    range: function
    render_axis_h: function
    render_axis_v: function
    render_bg: function
710    render_fg: function
    setup_data: function
    setup_layout: function
    setup_panel_guides: function
    setup_panel_params: function
715    setup_params: function
```

```
train_panel_guides: function
transform: function
super: <ggproto object: Class CoordCartesian, Coord, gg>
coord_params: list
720 facet: <ggproto object: Class FacetWrap, Facet, gg>
compute_layout: function
draw_back: function
draw_front: function
draw_labels: function
725 draw_panels: function
finish_data: function
init_scales: function
map_data: function
params: list
730 setup_data: function
setup_params: function
shrink: TRUE
train_scales: function
vars: function
735 super: <ggproto object: Class FacetWrap, Facet, gg>
facet_params: list
finish_data: function
get_scales: function
layout: data.frame
740 map_position: function
panel_params: list
panel_scales_x: list
panel_scales_y: list
render: function
745 render_labels: function
reset_scales: function
resolve_label: function
setup: function
setup_panel_guides: function
750 setup_panel_params: function
```

```
train_position: function  
super: <ggproto object: Class Layout, gg>
```

```
$plot
```

```
755
```

```
attr(,"class")  
[1] "ggplot_built"
```

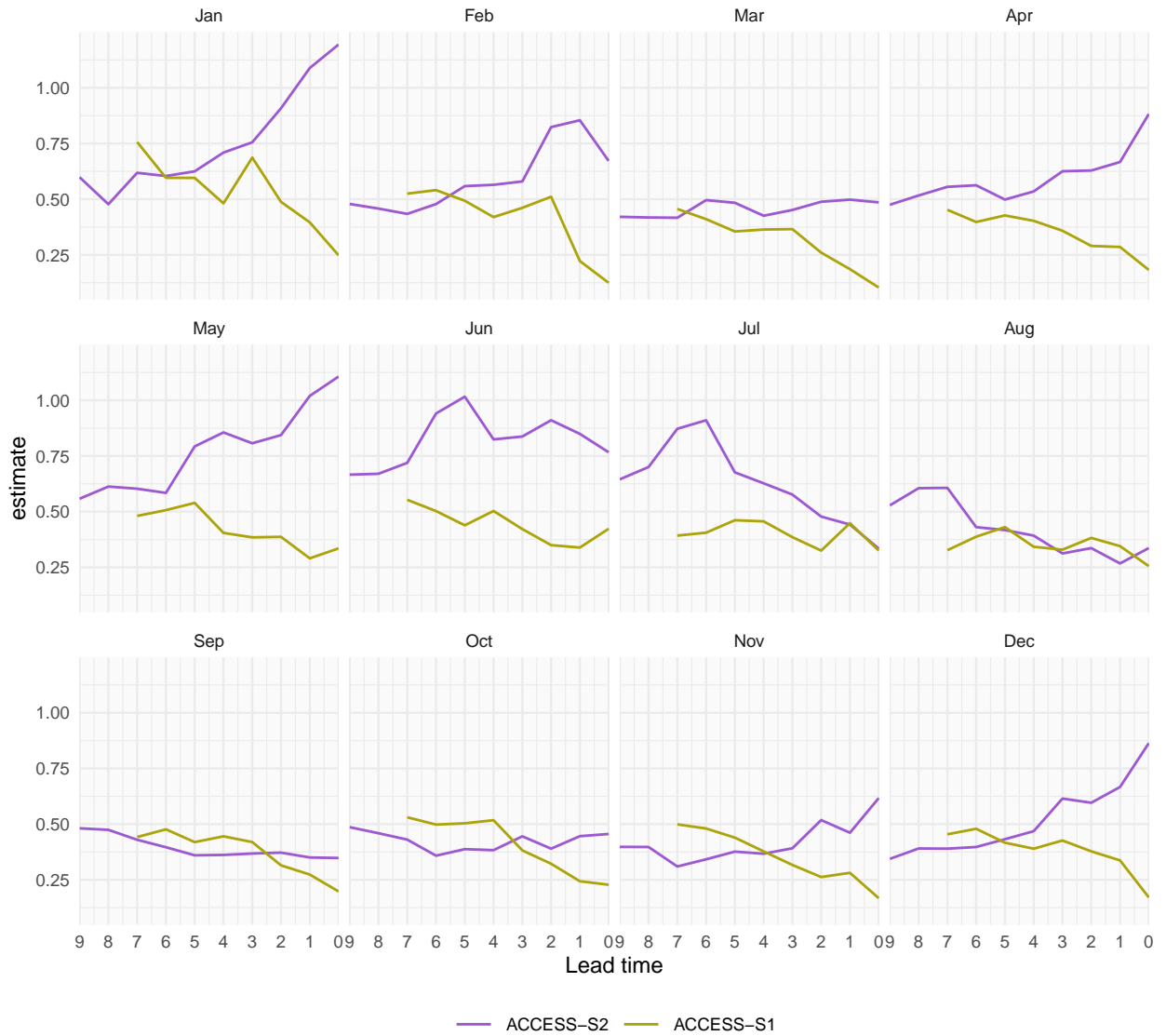


Figure A6. RMSE of monthly mean sea-ice extent anomalies as a function of lead time (months) for ACCESS-S1 (green) and ACCESS-S2 (purple). RMSE is computed over the overlapping period of ACCESS-S1 and ACCESS-S2 hindcasts (1990–2013). Each panel indicates the target month. Note the reverse horizontal axis.

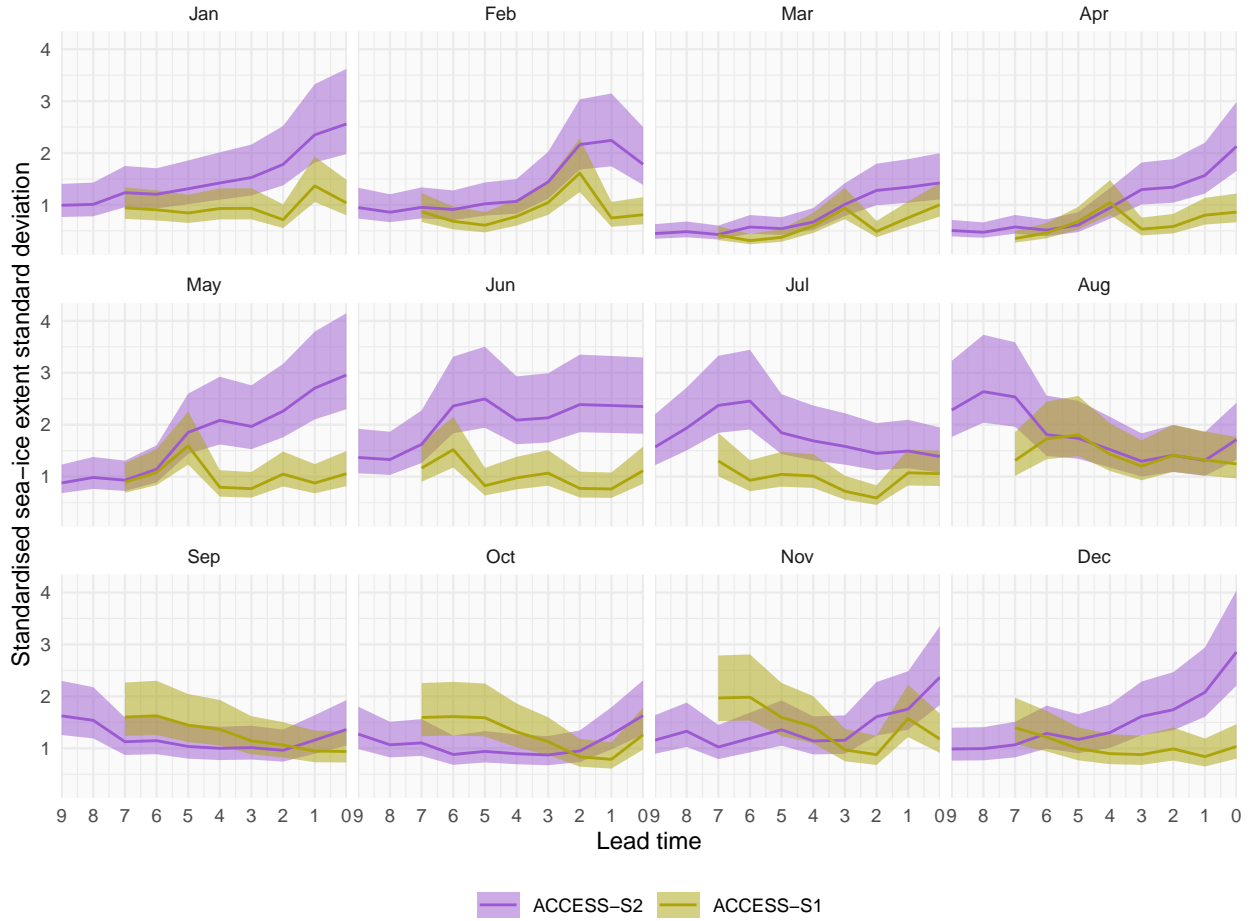


Figure A7. Interannual standard deviation with 95% confidence interval of monthly mean sea-ice extent forecasted for each month. We standardise the standard deviation by that month's sea-ice extent observation standard deviation. ACCESS-S1 and ACCESS-S2 at different lead times. Each panel indicates the target month. Note the reverse horizontal axis.

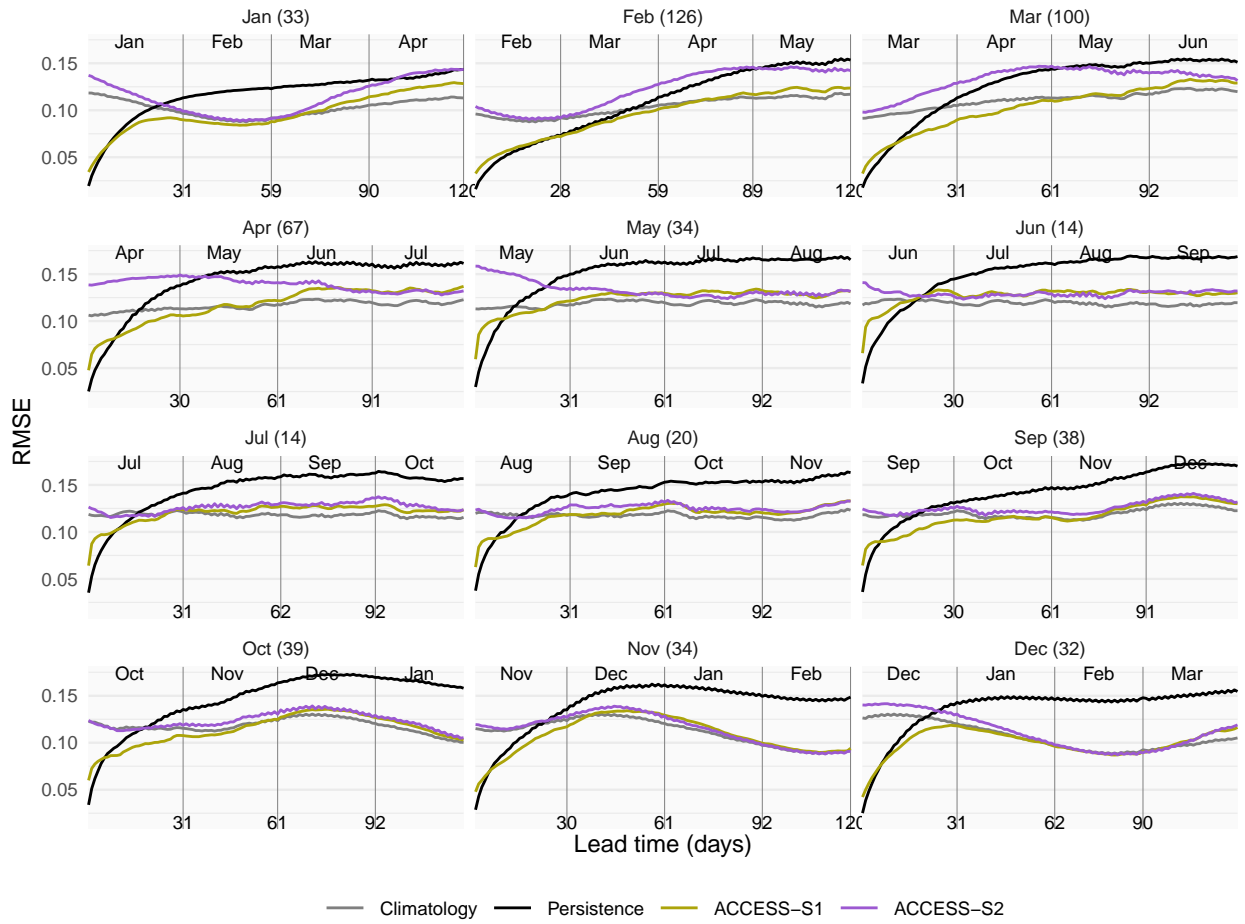


Figure A8. Mean RMSE of sea-ice concentration anomalies as a function of forecast lead time for all forecasts initialised on the first of each month compared with a reference forecast of persistence of anomalies (black) and climatology (gray). Only the first 120 days are shown. In parentheses, the shortest time at which ACCESS-S1 and ACCESS-S2 mean RMSE is not statistically different at the 99% confidence level.

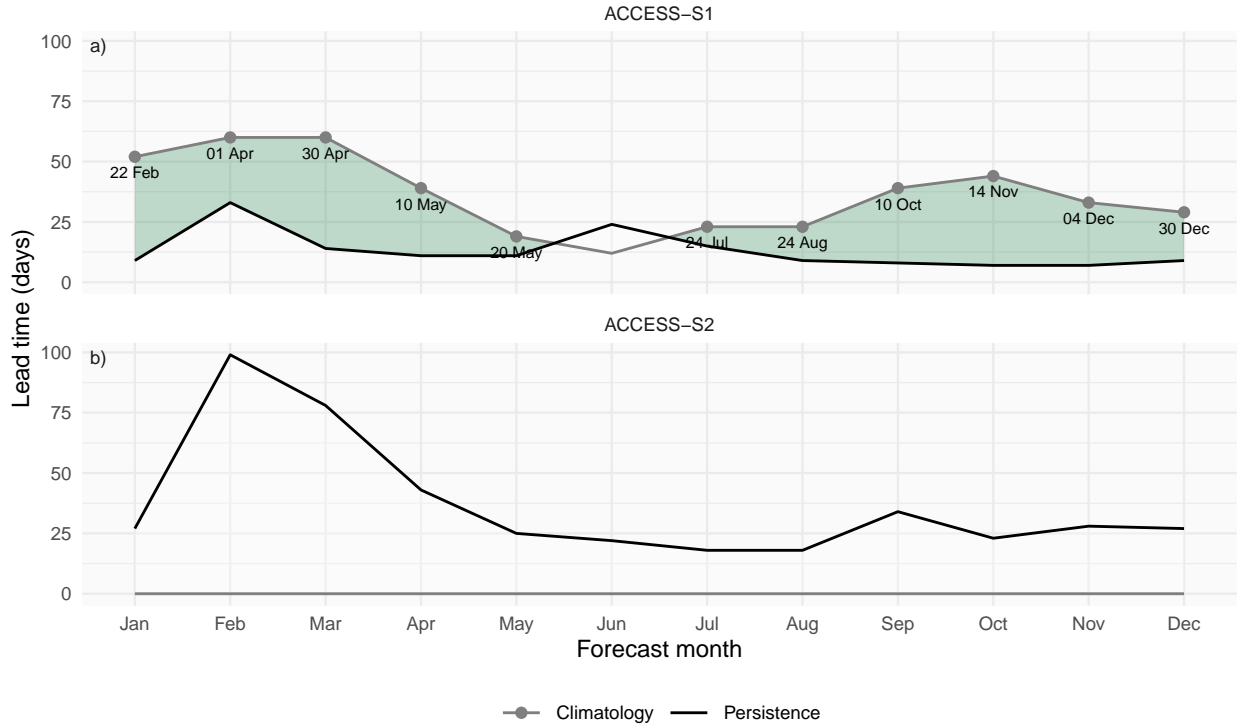


Figure A9. Minimum lead time at which each forecast's mean RMSE becomes larger than the lower bound of the 95% confidence interval of persistence forecast RMSE (black lines) and maximum lead time at which each forecast's mean RMSE remains lower than the lower bound of the 95% confidence interval of climatological forecast RMSE (gray line). Green shading indicates the window where forecasts outperform both persistence (lead times longer than black line) and climatology (lead times shorter than gray line). Text labels show the date corresponding to the maximum lead time at which each forecast outperforms climatology.

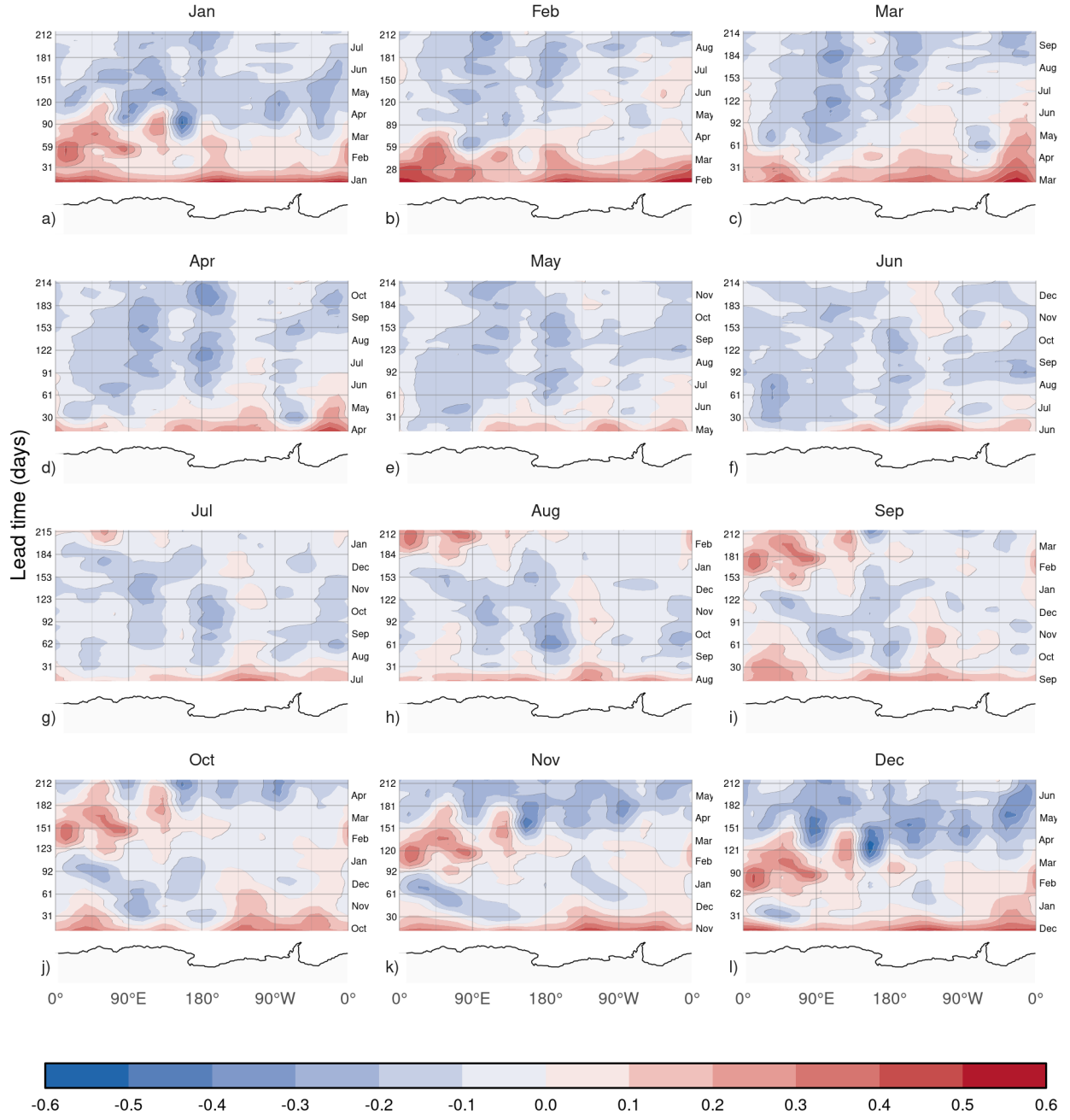


Figure A10. MSE skill score of ACCESS-S1 forecasts with climatological forecast as reference computed on 15 meridional slices 24° wide as a function of lead time and longitude. Antarctica's coastline is shown at the bottom of each panel for reference. Values were smoothed with an 11-day running mean to improve readability.

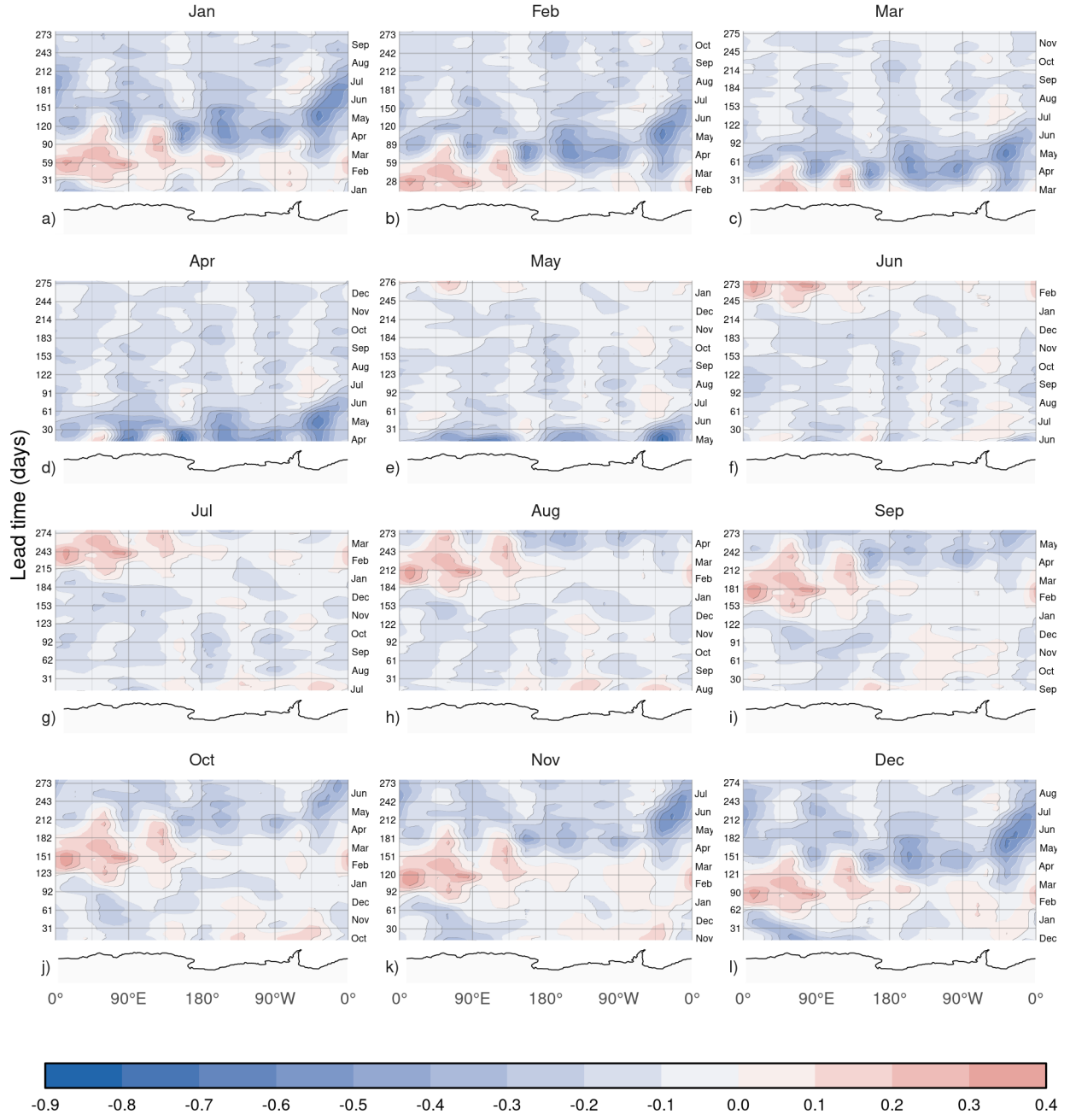


Figure A11. Same as Figure 11 but for ACCESS-S2.

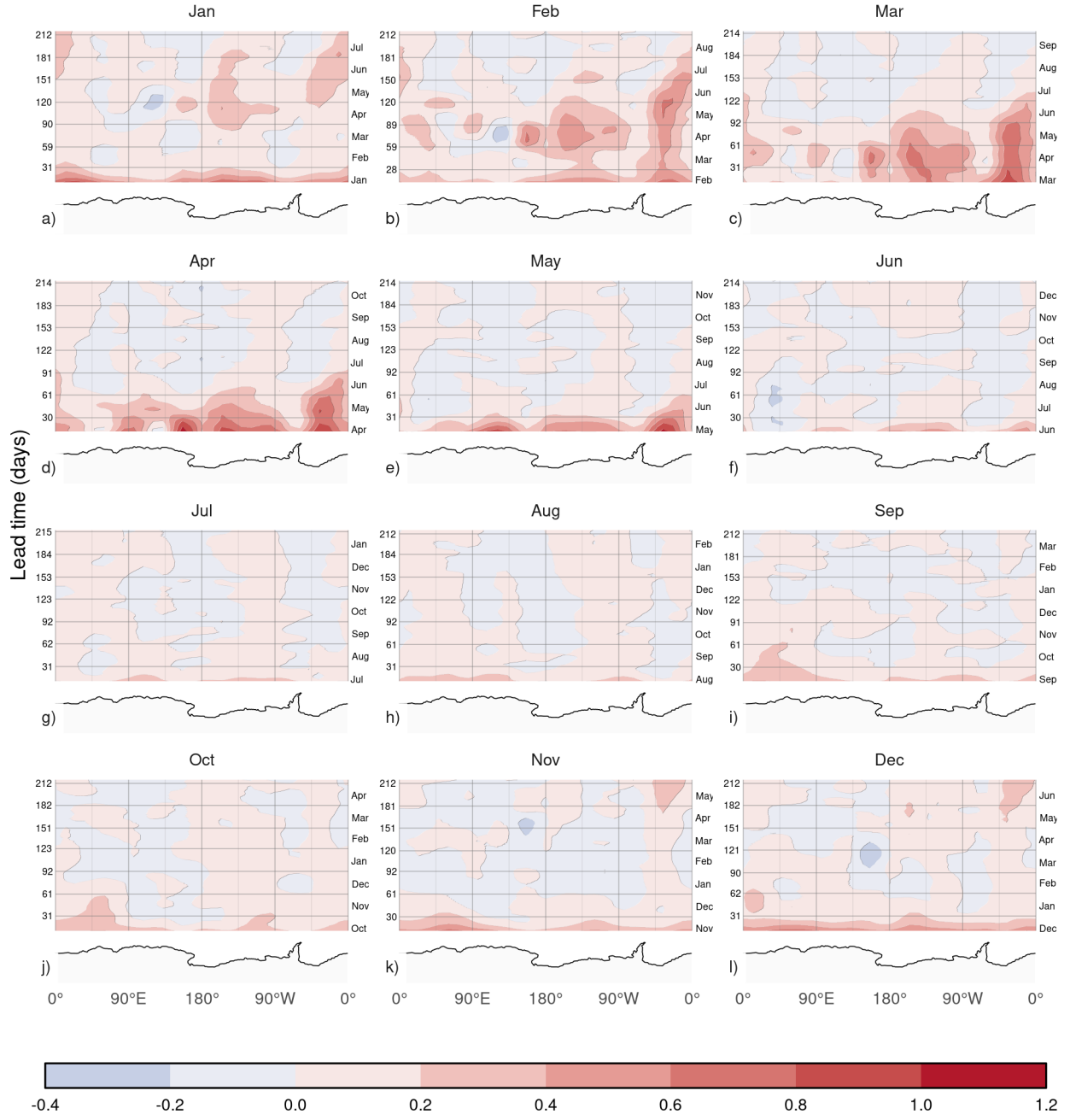


Figure A12. Same as Figure 11 but for the difference between ACCESS-S1 and ACCESS-S2.

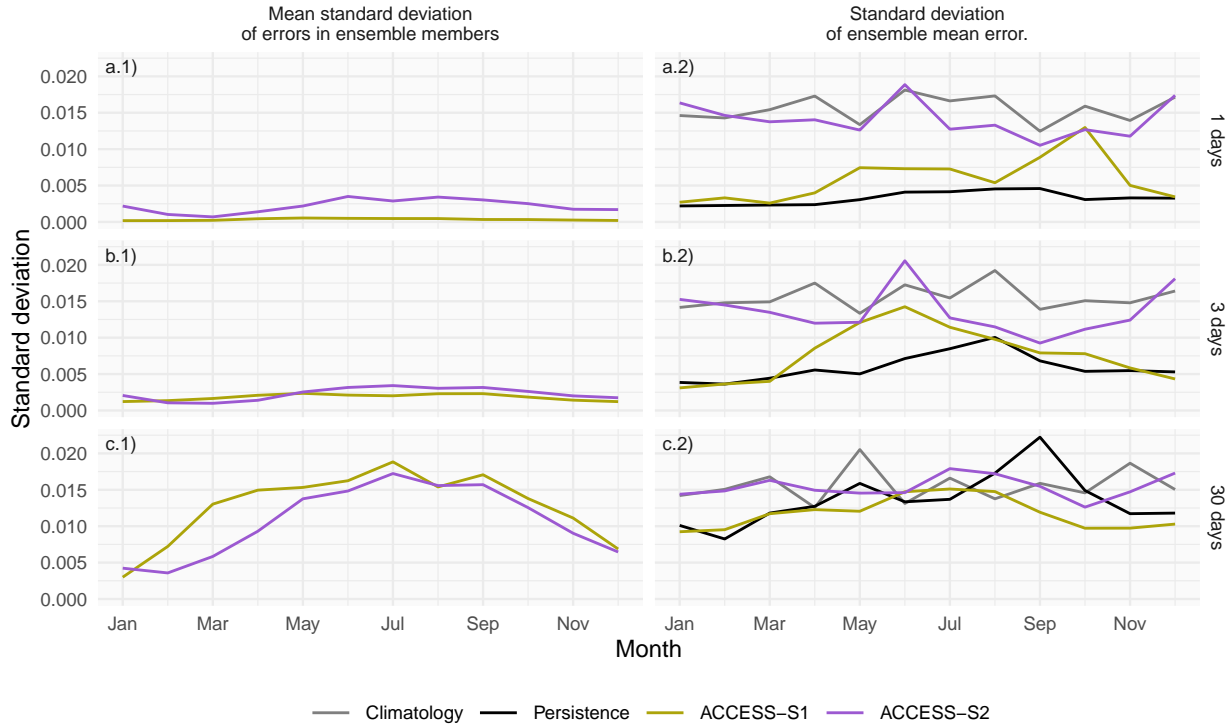


Figure A13. Decomposition of forecast error spread at 1, 5 and 30 days lead time for ACCESS-S1 and ACCESS-S2 hindcasts across initialization months. The left column shows the mean standard deviation of RMSE errors across ensemble members, while the right column shows the standard deviation of the ensemble mean RMSE error and the spread of the persistence and climatology forecasts errors.

B Code/Data availability

The underlying code for this study is available on GitHub: https://github.com/eliocamp/access-s2_ice-eval. Raw data of +S1 and +S2 hindcast are not available due to size. Derived datasets required to reproduce the results, including extent timeseries and error measures, are available in this Zenodo repository: <https://zenodo.org/records/17479538> ([Campitelli, 2025](#))

C Author contributions

EC performed the data analysis and wrote the manuscript draft. AP, JA, EL, MW and PR, performed interpretation of the results, and reviewed and edited the draft. All authors read and approved the final manuscript.

765 . D Competing interests

The authors declare no competing interests.

. E Acknowledgements

We thank the internal reviewers Bethan White and Xiaobing Zhou for their comments and feedback. This work benefited from earlier unpublished work by Laura Davies, Phil Reid, Andrew G. Marshall. This research was undertaken with the assistance
770 of resources from the National Computational Infrastructure (NCI Australia), an NCRIS enabled capability supported by the Australian Government. This work was supported by ARC SRIEAS Grant SR200100005 Securing Antarctica's Environmental Future.